J Comput Neurosci (2010) 28:247–266
DOI 10.1007/s10827-009-0202-2

Pseudo-Lyapunov exponents and predictability of Hodgkin-Huxley neuronal network dynamics

Yi Sun · Douglas Zhou · Aaditya V. Rangan · David Cai

Received: 16 May 2009 / Revised: 23 November 2009 / Accepted: 2 December 2009 / Published online: 18 December 2009

Abstract We present a numerical analysis of the dynamics of all-to-all coupled Hodgkin-Huxley (HH) neuronal networks with Poisson spike inputs. It is important to point out that, since the dynamical vector of the system contains discontinuous variables, we propose a so-called pseudo-Lyapunov exponent adapted from the classical definition using only continuous dynamical variables, and apply it in our numerical investigation. The numerical results of the largest Lyapunov exponent using this new definition are consistent with the dynamical regimes of the network. Three typical dynamical regimes—asynchronous, chaotic and synchronous, are found as the synaptic coupling strength increases from weak to strong. We use the pseudo-Lyapunov exponent and the power spectrum analysis of voltage traces to characterize the types of the network behavior. In the nonchaotic (asynchronous or synchronous) dynamical regimes, i.e., the weak or strong coupling limits, the pseudo-Lyapunov exponent is negative and there is a good numerical convergence of the solution in the trajectory-wise sense by using our numerical methods. Consequently, in these regimes the evolution of neuronal networks is reliable. For the chaotic dynamical regime with an intermediate strong coupling, the pseudo-Lyapunov exponent is positive, and there is no numerical convergence of the solution and only statistical quantifications of the numerical results are reliable. Finally, we present numerical evidence that the value of pseudo-Lyapunov exponent coincides with that of the standard Lyapunov exponent for systems we have been able to examine.

Keywords Lyapunov exponents · Hodgkin-Huxley neuron · Neuronal network · Chaos · Numerical analysis

Action Editor: David Terman

Y. Sun (✉) · D. Zhou · A. V. Rangan · D. Cai
Courant Institute of Mathematical Sciences,
New York University, New York, NY 10012, USA
e-mail: yisun@cims.nyu.edu

D. Cai
Department of Mathematics,
Shanghai Jiao Tong University,
Shanghai 200240, People's Republic of China

1 Introduction

Networks of conductance-based integrate-and-fire (I&F) neurons have been used to simulate the dynamics and study the properties of large scale neuronal networks (Somers et al. 1995; Troyer et al. 1998; McLaughlin et al. 2000; Cai et al. 2005; Rangan et al. 2005; Rangan and Cai 2007). But the I&F model does not account for the detailed generation of action potentials. We consider here the more physiologically realistic Hodgkin–Huxley (HH) model (Hodgkin and Huxley 1952; Dayan and Abbott 2001). This model of excitable membrane, originally introduced to describe the behavior of the squid's giant axon, provides a useful mechanism that accounts naturally for both the generation of spikes, due to voltage-dependent membrane conductances arising from ionic channels, and the existence of absolute refractory periods.

This classical model serves as the foundation for other neuron models with more complicated types of behavior, such as bursting. However, the complexity of the HH-like neuron model precludes detailed analytical studies of its quantitative properties, hence one often resorts to numerical simulations to study them.

In this work, we focus on the numerical investigation of HH neuronal network dynamics and describe how to characterize the types of the network's long time behavior (e.g., chaos) from the dynamical systems perspective. There have been extensive studies on the impact of chaos and the predictability of dynamical behaviors on biological and physical systems (Campbell and Rose 1983) and neuronal systems (Mainen and Sejnowski 1995; Hansel and Sompolinsky 1992, 1996; Kosmidis and Pakdaman 2003). Chaotic solutions have been observed in the study of a single HH neuron with different types of external inputs (Aihara and Matsumoto 1986; Guckenheimer and Oliva 2002; Lin 2006). In our study of all-to-all homogeneously coupled HH networks under a deterministic sinusoidal drive (Sun et al. 2009) or a stochastic Poisson input in this work, we find three typical dynamical regimes as the synaptic coupling strength varies. Under the external Poisson spike input, when the HH neurons are weakly coupled, the network is in an asynchronous state, where each neuron fires randomly with a train of spikes. When the coupling is relatively strong, the network operates in a synchronous state. For a moderately strong coupling between these two limits, the network dynamics exhibits chaotic behavior, as quantified by a positive Lyapunov exponent as well as a positive pseudo-Lyapunov exponent, as will be discussed below.

It turns out that there is a strong influence of the dynamical regimes on our numerical methods for evolving the network dynamics. In the nonchaotic dynamical regimes, i.e., the weak coupling or strong coupling limit, we show that there is a good numerical convergence of the solution in the classical, trajectory-wise sense by using our numerical methods. However, in the chaotic regime, i.e., with an intermediate strong coupling strength, there is no numerical convergence of the solution and only statistical quantifications of the numerical results are reliable. To characterize the chaotic/nonchaotic regimes, we employ several measures, such as measuring the pseudo-Lyapunov exponent and the power spectrum analysis of voltage traces, etc.

The largest positive Lyapunov exponent measures the rate of exponential divergence of perturbations of a dynamical system and it can be obtained by following two nearby trajectories with a separation which is of order ε, and calculating their average exponential rate of separation. For a *smooth* dynamical system in which all dynamical variables evolve continuously, there are standard algorithms to compute Lyapunov exponents (Parker and Chua 1989; Schuster and Just 2005). However, our HH network dynamics is a *nonsmooth* dynamics via pulse-coupled interactions, for which we use a second-order kinetic scheme to describe the dynamics of conductance. The conductance dynamics is described by an impulse response with the form of an α-function with both fast rise and slow decay timescales. The first derivative of the conductance dynamics of each neuron is discontinuous since its kinetic equation contains a Dirac δ-function that represents the arrival of the pulse induced by the presynaptic spikes or feed-forward spikes. If the trajectory vector contains the first derivative of the conductance dynamics when we calculate the separation between two trajectories, the separation can be of order one since at this moment it is possible that one trajectory may receive a spike but the other may not. Mueller examined how to extend the standard Lyapunov notion to dynamical systems with jumps (Mueller 1995). Here, we propose to examine the dynamics with jumps from a different point of view. We want to investigate the implication of jump dynamics for the flows in a subspace which contains all smooth variables. There is another motivation for our work: Can we predict the dynamics of the system by examining partial components of the system? For smooth dynamics without noise, the answer is yes. One can construct the so-called delay coordinate vectors to compute the largest Lyapunov exponent (Takens 1981). However, for nonsmooth dynamics, such as the HH neuronal networks we consider here, the answer is still not clear. Therefore, we define a *pseudo*-Lyapunov exponent adapted from the classical definition by excluding these discontinuous variables from the trajectory vector when we compute the separation rate of two nearby trajectories while using the standard method to measure the Lyapunov exponent (Parker and Chua 1989). Via numerical study, we demonstrate that the pseudo-Lyapunov exponent can capture the dynamical regimes of the network dynamics very well. As shown in our numerical study, the numerical values of the pseudo-Lyapunov exponents coincide with those of the standard Lyapunov exponents in the network systems for which we can employ standard methods to compute Lyapunov exponents. This indicates that classical results about Lyapunov exponents can be potentially extended to thresholded, pulse-coupled HH network dynamics.

The outline of the paper is as follows. In Section 2, we present a brief description of our HH neuronal

network model and the numerical method for evolving the network system. In Section 3, the definition of pseudo-Lyapunov exponents for the HH network system is described. In Section 4, we provide numerical results of several different HH neuronal networks, which illustrate the predictability of network dynamics from these pseudo-Lyapunov exponents. We present conclusions in Section 5.

2 The model

2.1 The network of Hodgkin-Huxley neurons

The dynamics of a Hodgkin-Huxley (HH) neuronal network with N neurons is governed by

$$C\frac{d}{dt}V_i = -G_{\mathrm{Na}}m_i^3h_i(V_i - V_{\mathrm{Na}}) - G_{\mathrm{K}}n_i^4(V_i - V_{\mathrm{K}}) - G_{\mathrm{L}}(V_i - V_{\mathrm{L}}) + I_i^{\mathrm{input}}, \tag{1}$$

$$\frac{dm_i}{dt} = \alpha_m(V_i)(1 - m_i) - \beta_m(V_i)m_i, \tag{2}$$

$$\frac{dh_i}{dt} = \alpha_h(V_i)(1 - h_i) - \beta_h(V_i)h_i, \tag{3}$$

$$\frac{dn_i}{dt} = \alpha_n(V_i)(1 - n_i) - \beta_n(V_i)n_i, \tag{4}$$

where the index i labels the neuron in the network, C is the cell membrane capacitance and V_i is its membrane potential, m_i and h_i are the activation and inactivation variables of the sodium current, respectively, and, n_i is the activation variable of the potassium current (Hodgkin and Huxley 1952; Dayan and Abbott 2001). The parameters G_{Na}, G_{K}, and G_{L} are the maximum conductances for the sodium, potassium and leak currents, respectively, V_{Na}, V_{K}, and V_{L} are the corresponding reversal potentials. Functional forms and parameters values for the HH neuron equations are given in Appendix A.

In our conductance-based network model, I_i^{input} stands for the synaptic input current, which is given by

$$I_i^{\mathrm{input}} = -\sum_{\mathrm{Q}} G_i^{\mathrm{Q}}(t)\left(V_i(t) - V_{\mathrm{G}}^{\mathrm{Q}}\right), \tag{5}$$

where $G_i^{\mathrm{Q}}(t)$ are the conductances with the index Q running over the types of conductances used, i.e., inhibitory and excitatory, and $V_{\mathrm{G}}^{\mathrm{Q}}$ are their corresponding reversal potentials (see Appendix A). The dynamics of $G_i^{\mathrm{Q}}(t)$ are governed by

$$\frac{d}{dt}G_i^{\mathrm{Q}}(t) = -\frac{G_i^{\mathrm{Q}}(t)}{\sigma_{\mathrm{r}}^{\mathrm{Q}}} + \widetilde{G}_i^{\mathrm{Q}}(t), \tag{6}$$

$$\frac{d}{dt}\widetilde{G}_i^{\mathrm{Q}}(t) = -\frac{\widetilde{G}_i^{\mathrm{Q}}(t)}{\sigma_{\mathrm{d}}^{\mathrm{Q}}} + \sum_{j\neq i}\sum_k S_{i,j}^{\mathrm{Q}}\delta\left(t - T_{j,k}^{\mathrm{S}}\right) + \sum_k F_i^{\mathrm{Q}}\delta\left(t - T_{i,k}^{\mathrm{F}}\right). \tag{7}$$

Each neuron is either excitatory or inhibitory, as indicated by its type $\mathscr{L}_i \in \{\mathrm{E}, \mathrm{I}\}$. There are two conductance types $\mathrm{Q} \in \{\mathrm{E}, \mathrm{I}\}$ also labeling excitation and inhibition. We say an action potential or emission of a spike occurs at time t if the membrane potential of a neuron (say the jth neuron of type Q) reaches a threshold value V^{th} at that time. Then the spike triggers postsynaptic events in all the neurons that the jth neuron is presynaptically connected to and changes their Q-type conductances with the coupling strengths $S_{i,j}^{\mathrm{Q}}$. On the other hand, for the postsynaptic ith neuron, its Q-type conductance $G_i^{\mathrm{Q}}(t)$ is determined by all spikes generated in the past from the presynaptic neurons of type Q. The term $\widetilde{G}_i^{\mathrm{Q}}(t)$ is an additional variable to describe the decay dynamics of conductance and the variable $G_i^{\mathrm{Q}}(t)$ has an impulse response with the form of an α-function with both a fast rise and a slow decay timescale, $\sigma_{\mathrm{r}}^{\mathrm{Q}}$ and $\sigma_{\mathrm{d}}^{\mathrm{Q}}$, respectively. The time $T_{j,k}^{\mathrm{S}}$ stands for the kth spike of neuron j prior to time t. The excitatory (inhibitory) conductance $\widetilde{G}^{\mathrm{E}}$ ($\widetilde{G}^{\mathrm{I}}$) of any neuron is increased when that neuron receives a spike from another excitatory (inhibitory) neuron within the network. This is achieved as follows: The coupling strengths $S_{i,j}^{\mathrm{E}}$ are zero whenever $\mathscr{L}_j = \mathrm{I}$, and similarly $S_{i,j}^{\mathrm{I}}$ are zero whenever $\mathscr{L}_j = \mathrm{E}$. For the sake of simplicity, we consider an all-to-all coupled neuronal network, in which $S_{i,j}^{\mathrm{Q}}$ is a constant $S^{\mathrm{Q}}/N^{\mathrm{Q}}$ with N^{Q} being the total number of Q-type neurons in the network. However, our method can readily be extended to more complicated networks with heterogeneous coupling strengths that can encode many different types of network architecture.

The system is also driven by feedforward inputs. Here we consider stochastic inputs: we use a spike train sampled from a Poisson process with rate r as the feedforward input. We denote $T_{i,k}^{\mathrm{F}}$ as the kth spike from the feedforward input to the ith neuron and it instantaneously increases that neuron's Q-type $\widetilde{G}_i^{\mathrm{Q}}(t)$ by magnitude F_i^{Q}. For simplicity, we also take F_i^{Q} to be a constant, F^{Q}, for Q-type conductance of all neurons in the network. The typical values or ranges of $\sigma_{\mathrm{r}}^{\mathrm{Q}}$, $\sigma_{\mathrm{d}}^{\mathrm{Q}}$, S^{Q} and F^{Q} can be found in Appendix A. For the numerical results reported here, we set $V^{\mathrm{th}} = -50\mathrm{mV}$.

The qualitative features of the network dynamics are insensitive to slight adjustments of the V^{th} value.

We note that, the conductance term $G_i^{\text{O}}(t)$ in Eq. (6) is a continuous function, but its first derivative is discontinuous, with a finite jump due to the presence of the Dirac δ-function in Eq. (7). This discontinuity in the network dynamics underlies our motivation for examining the pseudo-Lyapunov exponents and their implication in the classification of dynamical regimes of HH neuronal networks in the Section 3.

2.2 Numerical scheme

For network modeling, we need a stable and accurate numerical method to evolve the HH neuron equations coupled with the dynamics of conductances (Eqs. (1)–(7)) for each neuron. Since individual neurons interact with each other through conductance changes associated with presynaptic spike times, it is also necessary to have numerical interpolation schemes that can determine the spike times accurately and efficiently (Hansel et al. 1998; Shelley and Tao 2001). In our numerical study, we use the Runge-Kutta fourth-order scheme (RK4) with fixed time step for integrating the system, along with a cubic Hermite interpolation for estimating spike times. The whole scheme is fourth-order accurate. In Appendix B, Algorithm 1 details our numerical scheme for a single neuron.

When simulating the network dynamics, we need to carefully take into account the causality of spiking events within a single time step via spike-spike interactions, especially for large time steps (Rangan and Cai 2007). In some approaches with the traditional clock-driven strategy, like the modified Runge-Kutta methods (Hansel et al. 1998; Shelley and Tao 2001), at the beginning of a timestep, the state of the network at the end of the step is not known, thus, only the spikes of the feedforward input to the network within that time step can be used to attempt to evolve the system. This first approximation may indicate that, driven by the feedforward input spikes, many neurons in the network fire. However, this conclusion may be incorrect because the first few of these spikes induced within a large time step may substantially affect the rest of the network via spike-spike interactions in such a way that the rest of the spikes within the time step are spurious. For example, this happens when a large time step is used in these methods to evolve a network with strong recurrent inhibition. We note that the modified Runge-Kutta methods do not take into account spike-spike interactions within a single large numerical time step. As a consequence, when used to evolve a system with strong network coupling strengths, these methods need to take sufficiently small time steps to have only a few spikes in the entire system within a single time step. Here, we choose a strategy that allows for a larger time step, similar to the event-driven approach (Mattia and Del Giudice 2000; Reutimann et al. 2003; Rudolph and Destexhe 2007). We take the spike-spike correction procedure (Rangan and Cai 2007), which is equivalent to stepping through the sequence of all the synaptic spikes within one time step and computing the effect of each spike on all future spikes. We step through this correction process until the neuronal trajectories and spike times of neurons converge. Details of this spike-spike correction algorithm and the general coupling strategy are discussed in refs. (Rangan and Cai 2007; Sun et al. 2009). In Appendix C, Algorithm 2 details our numerical method for evolving the HH network model.

3 Lyapunov exponents

3.1 Smooth dynamics

A useful tool for characterizing chaos in a smooth dynamical system is the spectrum of Lyapunov exponents, in particular, the largest one, which measures the rate of exponential divergence or convergence from perturbed states of the system. A chaotic dynamics is signified by a positive largest Lyapunov exponent. Generally, the largest Lyapunov exponent λ can be obtained by following two sufficiently close nearby trajectories $\mathbf{X}(t)$ and $\mathbf{X}'(t)$ and calculating their average exponential rate of separation:

$$\lambda = \lim_{t\to\infty}\lim_{\varepsilon\to 0}\frac{1}{t}\ln\frac{\|\mathbf{Z}(t)\|}{\|\mathbf{Z}_0\|}, \tag{8}$$

where $\mathbf{Z}(t) = \mathbf{X}'(t) - \mathbf{X}(t)$, $\|\mathbf{Z}_0\| = \varepsilon$ and $\mathbf{Z}(0) = \mathbf{Z}_0$ is the initial separation. However, for a chaotic system, at least one Lyapunov exponent is positive. This implies that $\|\mathbf{Z}(t)\|$ grows unbounded as t becomes large. Therefore, a practical approach to avoid numerical overflows is to scale back one of the trajectories, say $\mathbf{X}'(t)$, to the vicinity of the other $\mathbf{X}(t)$ along the direction of separation whenever they become too far apart. We refer to this step as *renormalization* (Parker and Chua 1989; Schuster and Just 2005). Figure 1 illustrates the idea of this traditional algorithm. In this algorithm, one calculates the divergence of sufficiently close nearby trajectories after a finite time interval τ, and after each such interval, $\|\mathbf{Z}(n\tau)\|$ is renormalized to a fixed ε and separation rates after sufficiently many τ-intervals are

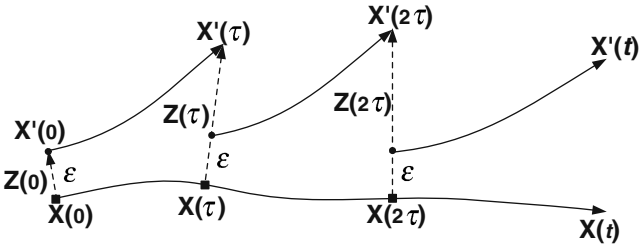

Fig. 1 Numerical evaluation of the largest Lyapunov exponent λ. Note that the dashed line represents the perturbation vector $\mathbf{Z}(t) = \mathbf{X}'(t) - \mathbf{X}(t)$. To avoid numerical overflows, after calculating the divergence of nearby trajectories at each step, $\|\mathbf{Z}(n\tau)\|$ is renormalized to the initial separation distance ε and the largest Lyapunov exponent is evaluated to be the average of separation rates after sufficiently many time intervals of length τ

averaged to obtain the largest Lyapunov exponent λ as follows,

$$\begin{aligned}
\mathbf{Z}(\tau) &= \mathbf{Z}(0)\exp(\lambda_1\tau);\\
\mathbf{Z}(2\tau) &= \mathbf{Z}(\tau)\frac{\varepsilon}{\|\mathbf{Z}(\tau)\|}\exp(\lambda_2\tau);\ldots.\\
\mathbf{Z}(k\tau) &= \mathbf{Z}((k-1)\tau)\frac{\varepsilon}{\|\mathbf{Z}((k-1)\tau)\|}\exp(\lambda_k\tau);\ldots. \qquad (9)
\end{aligned}$$

and

$$\lambda = \lim_{n\to\infty}\frac{1}{n}\sum_{k=1}^{n}\lambda_k = \lim_{n\to\infty}\frac{1}{n\tau}\sum_{k=1}^{n}\ln\frac{\|\mathbf{Z}(k\tau)\|}{\varepsilon}. \qquad (10)$$

In our simulation, we take $\varepsilon = 10^{-8}$, which is sufficiently small for estimating λ. We have verified that slightly larger ε values yield the same results as reported here. The selection of the value of τ is determined by the following considerations: too small a value of τ leads to an excessive number of renormalizations, resulting in ratios $\frac{\|\mathbf{Z}(k\tau)\|}{\varepsilon}$ which are all nearly one, thus, giving rise to numerical inaccuracies in the calculation; too large a value of τ could lead to numerical overflows in the integration of the trajectories (Parker and Chua 1989). In the numerical results shown in Section 4, we will present a convergence test of the largest Lyapunov exponent using different values of τ. These values range from the length of the time step used for evolving the trajectories to a maximum value 50 ms and they produce convergent results. We emphasize that the Lyapunov exponents are a statistical property of a full dynamical system (Ott 1993). Even if our numerically obtained trajectories are not convergent in a chaotic regime, we did, however, verify that our Lyapunov exponent computation indeed exhibits convergence as the time steps used to compute the trajectories become smaller and smaller.

3.2 Pseudo-Lyapunov exponents

There are two main motivations for us to propose the so-called pseudo-Lyapunov exponents. The first one is as follows. In many applications, one cannot always obtain all the components of the vector giving the state of the dynamical system and the only available information of the system is one or a few measured scalar time series, e.g., the data of the membrane potential of individual neurons. In such a situation, can we characterize and predict the dynamics of the system? For smooth dynamics without noise, the answer is yes. For example, given a measured scalar time series $u(t)$, one can construct the so-called delay coordinate vector (Takens 1981), an d-dimensional vector of the following form: $\mathbf{U}(t) = (u(t), u(t+\tau), \ldots, u(t+(d-1)\tau))$, to represent the original dynamical system, where τ is the delay time and d is the embedding dimension. It has been proven that for properly chosen τ, if the embedding dimension is sufficiently large, say, at least more than twice the dimension D of the attractor of the system, i.e., $d > 2D+1$, then generically there exists a diffeomorphism between the reconstructed and the original attractors (Takens 1981). Therefore, one can consider to use partial components in the vector $\mathbf{X}(t)$ to compute the largest Lyapunov exponent. However, for nonsmooth dynamics, such as the HH networks we consider here, Takens' theorem no longer holds. The question of how much information we can extract by examining partial components of the system remains open.

The second motivation of invoking pseudo-Lyapunov exponents is to attempt to circumvent the difficulties in evaluating standard Lyapunov exponents arising from the nonsmooth variables in the vector $\mathbf{X}(t)$. The algorithm described in the previous subsection for evaluating the largest Lyapunov exponent is designed for a smooth dynamical system, in which all dynamical variables evolve continuously. By performing the renormalization procedures, one can always keep the separation between the nearby trajectories within order ε. However, as evident in Eq. (7), the dynamical variable $\widetilde{G}_i^{\mathrm{Q}}$ of each neuron is discontinuous since its kinetic equation contains a δ-function that represents the pulse induced by the presynaptic spikes or feedforward spikes. When one calculates the separation between two trajectories and performs the renormalization, one trajectory of the entire network may receive a spike but the nearby trajectory may not, which induces an order one difference in the dynamics of $\widetilde{G}_i^{\mathrm{Q}}$ between two trajectories. Figure 2 illustrates this situation. Mueller showed that a generalized method can be applied to calculate the Lyapunov exponents

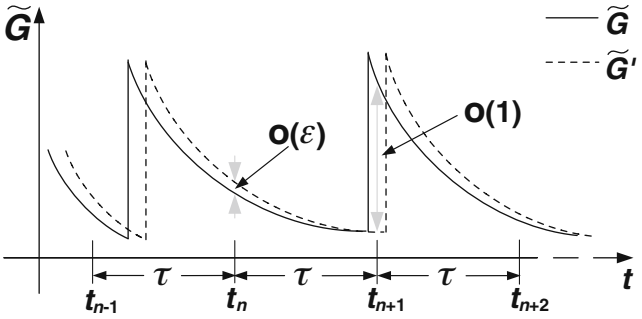

Fig. 2 Divergence in the conductance term $\widetilde{G}_i^{\mathrm{Q}}$ between two trajectories. We calculate the separation between two trajectories and do the renormalization at each time step $t_n = n\tau$. Note that at time t_n, the separation is of order ε. However, at time t_{n+1}, the neuron in the trajectory $\mathbf{X}(t)$ has already received a synaptic spike and its conductance term $\widetilde{G}_i^{\mathrm{Q}}$ is increased by coupling strength S^{Q}, which is of order one, but the neuron in the nearby trajectory $\mathbf{X}'(t)$ has not received a spike yet. Therefore, the separation is of order one, which can induce errors in the calculation of largest Lyapunov exponent

by taking care of handling the discontinuities and supplementing transition conditions at the instants of discontinuities (Mueller 1995). In numerical computation of the Lyapunov exponents, instead of using transition conditions, we can wait to calculate the separation between two trajectories until the next renormalization time step point after the time interval τ when both trajectories pass the discontinuity points. But we also note that when the size of network N is very large, the number of firing events increases, then the number of the discontinuity points increases and this situation can make the waiting time too long and numerical overflows again become a problem since we need to wait for all neurons in both trajectories to pass their discontinuity points. However, by taking the perturbation amplitude ε sufficiently small, we may reduce the probability of these situations to occur.

Here, we propose to examine the dynamics with discontinuities from a different point of view. We want to investigate the implication of jump dynamics for the flows in a subspace which contains all smooth variables. For this aim, we propose a pseudo-Lyapunov exponent adapted from the traditional definition. When we calculate the separation of two nearby trajectories to measure the largest Lyapunov exponent, we simply include only those variables that are continuous from the trajectory vector. Hence, the variable $\widetilde{G}_i^{\mathrm{Q}}$ is excluded in our present case, i.e., we only consider:

$$X_i(t) = \left(V_i(t), m_i(t), h_i(t), n_i(t), G_i^{\mathrm{Q}}(t)\right) \tag{11}$$

for each neuron and use the vector $\mathbf{X}(t) = [X_1(t), \ldots, X_i(t), \ldots, X_N(t)]$ to characterize the dynamics of the entire network. As shown in Section 4, the numerical results of the largest pseudo-Lyapunov exponent evaluated using this projection to the smooth part of the dynamics are consistent with the dynamical regimes of the network as characterized by other quantifications.

In summary, we evaluate the largest pseudo-Lyapunov exponent as follows: at the initial time $t_0 = 0$, for the original trajectory point $\mathbf{X}(0)$, we select a nearby point $\mathbf{X}'(0)$ with the initial separation distance $\|\mathbf{Z}(0)\| = \varepsilon$; then we advance both trajectories to τ and calculate the new separation $\|\mathbf{Z}(\tau)\|$ to evaluate the exponential rate of separation:

$$\lambda_1 = \frac{1}{\tau} \ln \frac{\|\mathbf{Z}(\tau)\|}{\varepsilon}; \tag{12}$$

meanwhile, the nearby trajectory $\mathbf{X}'(\tau)$ is renormalized so the separation is ε in the same direction as $\mathbf{Z}(\tau)$:

$$\mathbf{Z}(\tau) \leftarrow \mathbf{Z}(\tau) \frac{\varepsilon}{\|\mathbf{Z}(\tau)\|}; \tag{13}$$

Then we repeat these procedures to obtain $\lambda_2, \ldots, \lambda_k$ and calculate the average of the exponential rate of separation by using Eq. (10).

4 Results

4.1 Three dynamical regimes of the network

First, we consider an all-to-all coupled network of 100 excitatory neurons driven by a feedforward input, which is a realization of a Poisson process with the rate $\omega = 50$ Hz. Other parameters are given in Appendix A. We perform simulations of this network for synaptic coupling strength S ranging from 0.025 to 1.0 mS/cm^2 with an increment of $\Delta S = 0.025$ mS/cm^2. A systematic scanning result of the pseudo-Lyapunov exponents obtained by using our method over a long time interval of $T = 2^{16} = 65536$ ms is shown in Fig. 3(a–c). As illustrated below, the result reveals three typical dynamical regimes—an asynchronous, a chaotic, and a synchronous regime. The "chaotic" regime of the network exists in $0.263 \lesssim S \lesssim 0.395$ mS/cm^2 in the sense that the pseudo-Lyapunov exponent is positive in this range (We will further characterize this regime by other quantifications). The left part ($0.025 \lesssim S \lesssim 0.263$ mS/cm^2) and the right part ($0.395 \lesssim S \lesssim 1.0$ mS/cm^2) correspond to the asynchronous state and synchronous state, respectively.

(i) Asynchronous state For very small values of the coupling strength, the drive to a single neuron due to the presynaptic spikes is so weak that the dynamics of each neuron is essentially driven by the feedforward

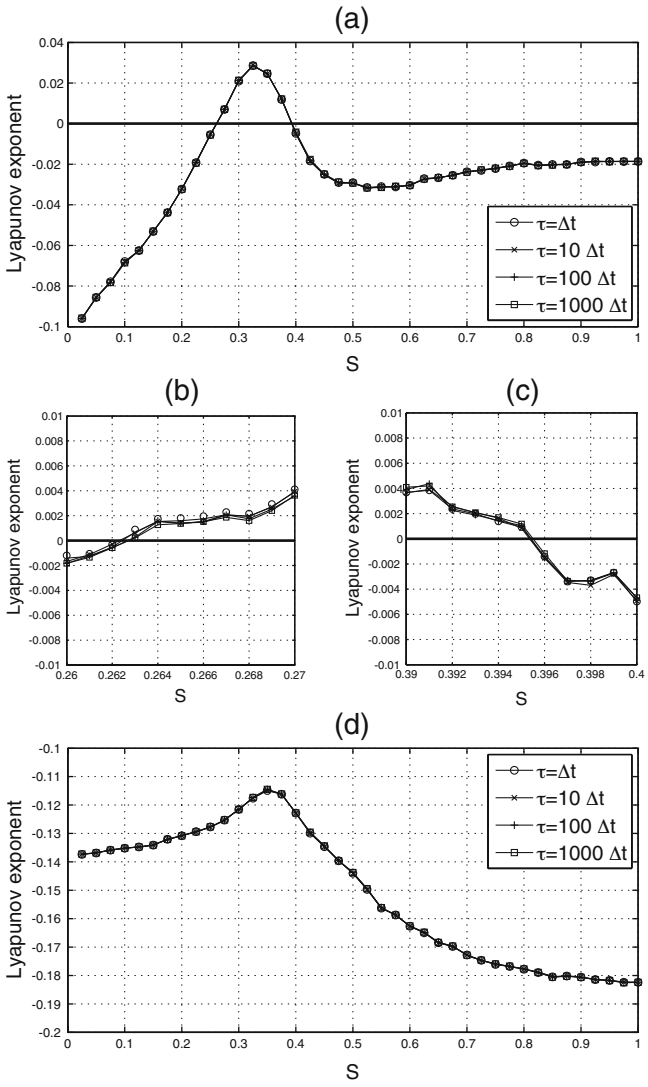

Fig. 3 (**a**): The pseudo-Lyapunov exponent versus the coupling strengths S. The network is all-to-all coupled with 100 excitatory neurons driven by a feedforward input, which is a realization of a Poisson process with the rate $\omega = 50$ Hz; (**b**): A fine scanning result on [0.26, 0.27] mS/cm^2. (**c**): A fine scanning result on [0.39, 0.40] mS/cm^2. (**d**): The pseudo-Lyapunov exponent of a single test neuron (see text) in the network versus the coupling strengths S. In each plot the time step Δt for the RK4 solver is fixed to 2^{-5} ms and we use different renormalization time interval τ from Δt to $1000\Delta t$ to evaluate the pseudo-Lyapunov exponent. The results here indicate our pseudo-Lyapunov exponent calculation has achieved a numerical convergence. Note that all the curves for different values of τ essentially overlap. The total time of the trajectories is sufficiently long (65536 ms) in order to obtain statistically convergent results for the pseudo-Lyapunov exponent

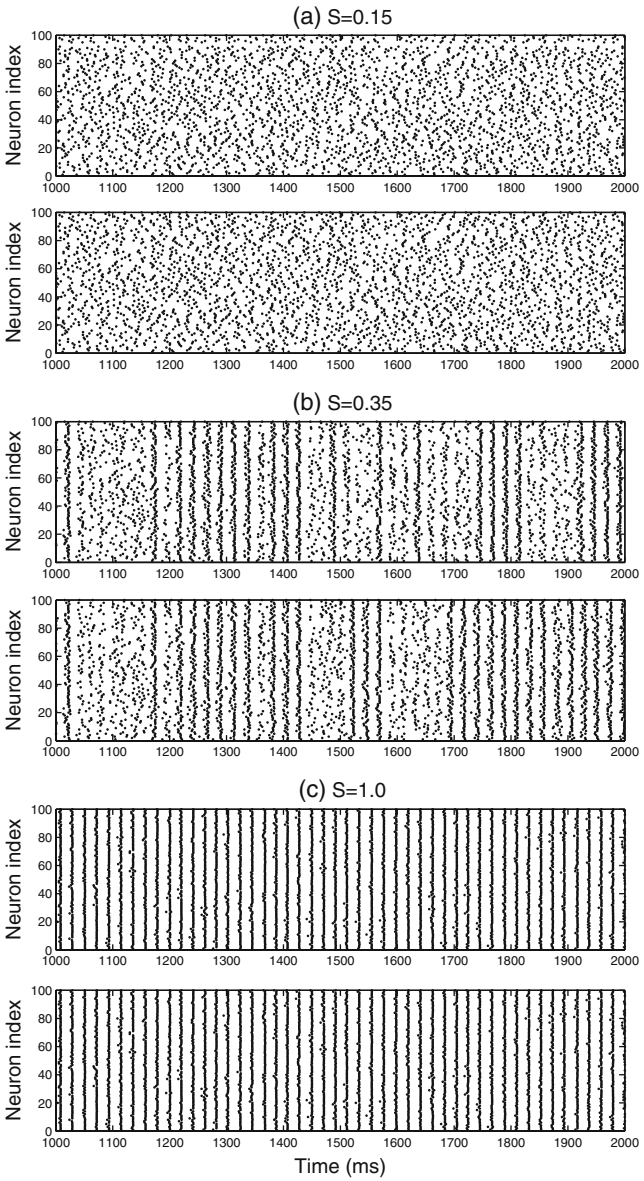

Fig. 4 Raster plots of spike events in the same network as the one in Fig. 3 computed using different time steps with same initial conditions. The plots from (**a**) to (**c**) show typical cases of three dynamical regimes with the coupling strength $S = 0.15$, 0.35, and 1.0 mS/cm^2, respectively: (**a**) Asynchronous dynamics; (**b**) Chaotic dynamics; (**c**) Synchronous dynamics. In each case we show two simulation results obtained by using different time steps $\Delta t = 2^{-5}$ (upper) and 2^{-4} ms (lower), respectively

input and the neurons fire at random, as is expected. Two raster plots of the case $S = 0.15$ mS/cm^2 obtained by using two different time steps $\Delta t = 2^{-5}$ and 2^{-4} ms with same initial conditions are shown in Fig. 4(a). It can clearly be seen that the computed trajectories cannot be distinguished from each other and the firing times are reliable. This type of *asynchronous* states exists for $0.025 \lesssim S \lesssim 0.263$ mS/cm^2.

This case is also characterized by the power spectra. We computed two kinds of power spectra: (1) the mean power spectrum, averaged over all neurons, of membrane potential trace, and (2) the power spectrum of the mean membrane potential trace averaged over

all neurons (Fig. 5(a)). Both of the power spectra are of broad-band, with an asymptotic $\sim \omega^{-2}$ decay at high frequencies, signifying that (1) there are no clear oscillations in the dynamics and (2) there is an exponential decay of time-correlations of the measured quantities, as implied by the Wiener-Khinchin theorem.

Moreover, we can verify the accuracy of our numerical method by performing convergence tests of the numerical solutions. For each test, we obtain a high precision solution at time $t = 1024$ ms with a time step ($\Delta t = 2^{-16} \approx 1.5 \times 10^{-5}$ ms) which is sufficiently small so that the solutions using the algorithm with or without spike-spike corrections produce the same convergent solution. We take the convergent solution as a representation of the high precision solution $\mathbf{X}^{\text{high}}(t)$. Here, for simplicity of notation, we use the same definition of solution vector as Eq. (11) with $\mathbf{X}(t) = [X_1(t), \ldots, X_i(t), \ldots, X_N(t)]$ to represent the solution of entire network. We compare the high precision solution $\mathbf{X}^{\text{high}}(t)$ with the trajectories $\mathbf{X}^{\Delta t}(t)$ calculated with larger time steps $\Delta t = 2^{-9} \to 2^{-4}$ ms. We measure the numerical error in the L^2-norm as follows:

$$E = \left\| \mathbf{X}^{\Delta t} - \mathbf{X}^{\text{high}} \right\|. \tag{14}$$

As shown in Fig. 6, our method can achieve fourth-order numerical convergence for $S = 0.15$ mS/cm^2, which is consistent with the fact that the pseudo-Lyapunov exponent is measured to be negative (Fig. 3(a)).

(ii) Chaotic state For intermediate coupling strength, in this network for $0.263 \lesssim S \lesssim 0.395$ mS/cm^2, sometimes the neurons fire at random in an asynchronous way and sometimes they fire in an almost synchronous way. In Fig. 4(b) of the case $S = 0.35$ mS/cm^2, two raster plots obtained by using two small time steps $\Delta t = 2^{-5}$ and 2^{-4} ms with same initial conditions exhibit a marked difference in spiking patterns of neurons and the firing times seem to be unreliable and very sensitive to numerical time steps even if they are sufficiently small. As shown in Fig. 6, the convergence test indicates that we cannot achieve expected numerical convergence of the solutions for this case. Moreover,

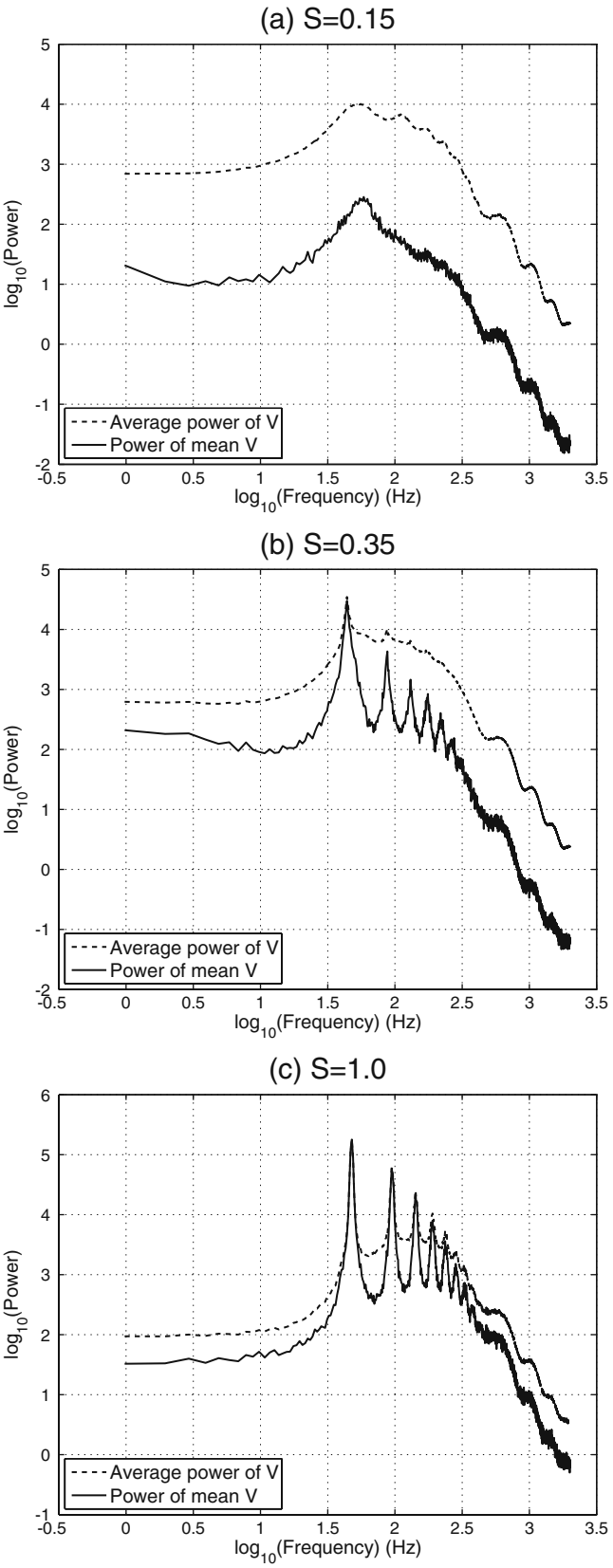

Fig. 5 The power spectrum of membrane potential trace of the neurons in the same network as the one in Fig. 3. The plots from (**a**) to (**c**) show three cases with the coupling strength $S = 0.15$, 0.35, and 1.0 mS/cm^2 corresponding to an asynchronous, chaotic and synchronous regime, respectively. In each plot the *upper (dashed) line* corresponds to the mean power spectrum, averaged over all neurons, of a neuron's membrane potential trace; the *lower (solid) line* represents the power spectrum of the mean membrane potential trace averaged over all neurons

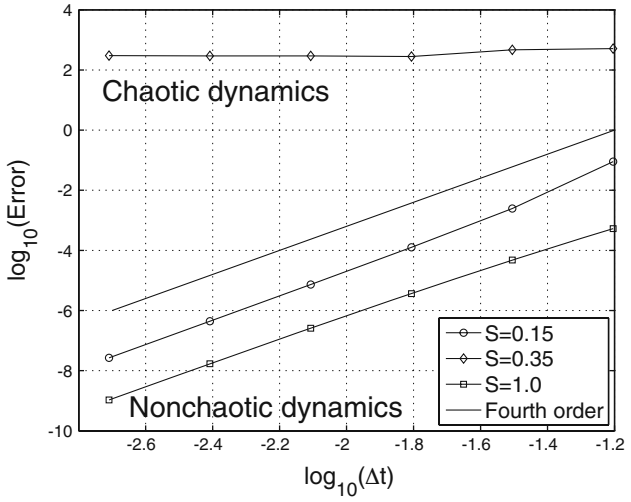

Fig. 6 The convergence tests are performed on the same network as the one in Fig. 3 by using the RK4 scheme with a final time of $t = 1024$ ms. In the plot we show three cases with the coupling strength $S = 0.15$ (*circles*), 0.35 (*crosses*) and 1.0 mS/cm^2 (*squares*), respectively. The *solid line* indicates the slope for the fourth order convergence

the statistical results for long time simulation show that the dynamics of the network is *chaotic* in the sense that the pseudo-Lyapunov exponent is measured to be positive, as shown in Fig. 3(a). As will be reported below, in our numerical study, we have also shown that the pseudo-Lyapunov exponents as we defined here coincided with the standard Lyapunov exponents for the network dynamics that we can examine numerically. Therefore, chaotic dynamics in the sense of a positive largest Lyapunov exponent is captured by our pseudo-Lyapunov exponent.

The mean power spectrum, averaged over all neurons, of a neuron's membrane potential trace in Fig. 5(b) also has a broad-band nature with small peaks. The power spectrum of this chaotic state is similar to that of the asynchronous state (Fig. 5(a)). However, there are weak peaks in the spectra, typical of a chaotic dynamics, in which oscillations coexist with irregular time dynamics (Schuster and Just 2005). It is interesting to note that the power spectrum of the mean membrane potential trace averaged over all neurons contains stronger, broad peaks, indicating weak coherent, synchronous oscillations in the dynamics, as evidenced in Fig. 4(b). It appears that the mean membrane potential averaged over all neurons can detect more efficiently the underlying oscillations in the system.

(iii) Synchronous state When the coupling is strong, $S \gtrsim 0.395$ mS/cm^2, a large portion of neurons in the network fire synchronously after a few of the neurons fire in advance. This firing pattern is shown in two raster plots in Fig. 4(c) for the case $S = 1.0$ mS/cm^2 obtained by using two different time steps $\Delta t = 2^{-5}$ and 2^{-4} ms with same initial conditions. The raster patterns are identical within the numerical accuracy and the firing times are reliable in the sense that they are not sensitive to numerical simulation time steps as long as they are sufficiently small. Figure 6 also shows that our method can achieve fourth-order numerical convergence when $S = 1.0$ mS/cm^2, which is consistent with the corresponding pseudo-Lyapunov exponent being negative (Fig. 3(a)), as commented above.

As shown in Fig. 5(c), both of the power spectra contain peaks clearly located at integer multiples of the fundamental frequency 50 Hz, indicating that the membrane potential evolves with a strong periodical component consistent with the feedforward input rate 50 Hz and the neurons fire almost synchronously, as seen in Fig. 4(c).

In addition to the three typical dynamical regimes, we also present the results of two special cases ($S = 0.263$ and 0.395 mS/cm^2) to show the transitions from the asynchronous state to the chaotic state and from the chaotic state to the synchronous state, respectively. A raster plot of the first case $S = 0.263$ mS/cm^2 is shown in Fig. 7(a). A large portion of neurons in the network still fire at random and the mean power spectrum, averaged over all neurons, of a neuron's membrane potential trace in Fig. 7(b) has a broad-band nature, which is similar to that of the asynchronous state (Fig. 5(a)). However, for this coupling strength, the drive to a single neuron due to the presynaptic spikes reaches a certain level so that some small clusters of neurons in the network start to fire synchronously. Moreover, the power spectrum of the mean membrane potential trace averaged over all neurons (Fig. 7(b)) contains a stronger, broad peak, around the fundamental frequency 50 Hz indicating weak coherent, synchronous oscillations in the dynamics.

A raster plot of the second case $S = 0.395$ mS/cm^2 is shown in Fig. 7(c). Most of time the neurons fire in an almost synchronous way, but there are still time periods when they fire at random in an asynchronous way. As shown in Fig. 7(d), both of the power spectra are similar to those of the chaotic state (Fig. 5(b)). The mean power spectrum, averaged over all neurons, of a neuron's membrane potential trace also has a broad-band nature with weak peaks, which indicates that oscillations coexist with irregular time dynamics. The power spectrum of the mean membrane potential trace averaged over all neurons contains stronger, broad peaks, indicating weak coherent, synchronous oscillations in the dynamics.

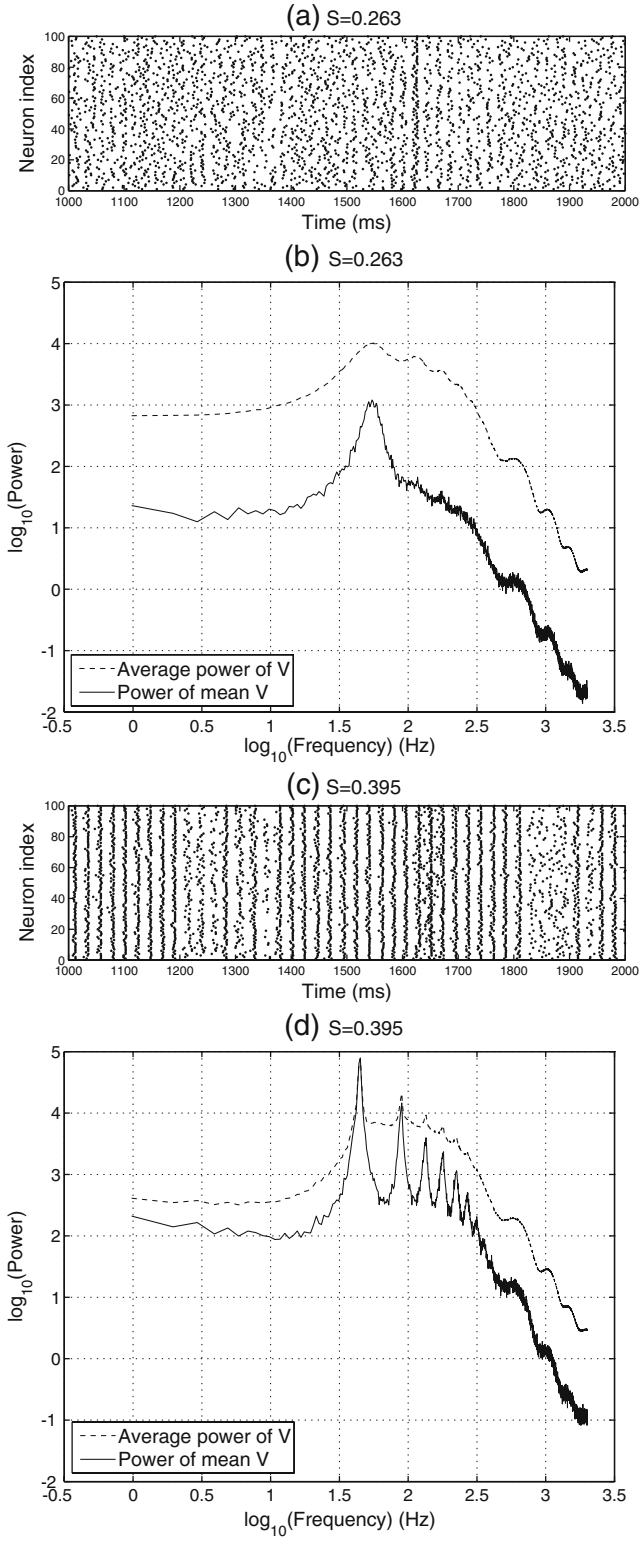

Fig. 7 (**a**–**b**) Raster plot of spike events and the power spectrum of membrane potential trace of the neurons in the same network as the one in Fig. 3 with the coupling strength $S = 0.263$ mS/cm^2, respectively. (**c**–**d**) Raster plot and the power spectrum for the case of $S = 0.395$ mS/cm^2, respectively

It has been shown that chaos can arise in the dynamics of a single HH neuron, for example, under a periodic external drive (Guckenheimer and Oliva 2002; Lin 2006). On the other hand, in some *in vitro* experiments it was found that single neurons are reliable under a broad range of conditions, i.e., the spike times of a neuron *in vitro* in response to repeated injections of a fixed, fluctuating current signal tend to be repeatable across multiple trials (Mainen and Sejnowski 1995). Therefore, there is a natural question: what about a single neuron in the HH network under a stochastic external Poisson input and the inputs from other neurons, can it be chaotic?

To address whether the dynamics of a neuron that receives the feedforward input plus the spikes from other neurons in the network, can be chaotic or not, we introduce the notion of a "test" neuron. For example, if we want to examine the dynamics of the ith neuron with its trajectory $X_i(t)$ in the network, we create a test neuron, whose trajectory $X_i'(t)$ is close to $X_i(t)$. This test neuron $X_i'(t)$ receives the same feedforward input plus the same synaptic spikes from other neurons in the network as the ith neuron $X_i(t)$ does. But we do not feed the output spikes generated by this test neuron $X_i'(t)$ back into the network. Then we can calculate the pseudo-Lyapunov exponent λ_i for the dynamics of the ith neuron by following $X_i(t)$ and $X_i'(t)$ with the same integration and renormalization procedures for sufficiently long time as we describe for computing the pseudo-Lyapunov exponent of the network dynamics in Subsection 3.2. The initial separation ε between $X_i(t)$ and $X_i'(t)$ is also set to 10^{-8}, which is sufficiently small for estimating the pseudo-Lyapunov exponent. We have verified that slightly large ε values yield the same results as reported here. Figure 3(d) shows the numerical results for the same range of S as in Fig. 3(a). The pseudo-Lyapunov exponent of a single neuron remains negative for any value of S. We have also verified that the pseudo-Lyapunov exponent of other single neurons are all negative. This result indicates that the dynamics of a single neuron in the network in the sense of test neurons is not chaotic. The chaos is a phenomenon under the effect of a *network* dynamics with feedback of every neuron to other neurons.

4.2 Attractor structures of the network dynamics

As we mentioned in Subsection 3.2, it is possible to use partial components in the vector $\mathbf{X}(t)$ to compute the largest Lyapunov exponent. If the unstable directions in individual dynamic subspaces $\mathbf{V}(t) = [V_1(t), \ldots, V_i(t), \ldots, V_N(t)]$, $\mathbf{m}(t)$, $\mathbf{h}(t)$, $\mathbf{n}(t)$, (defined similarly as $\mathbf{V}(t)$) are not perpendicular to

each other in phase space, the expansion or contraction rate along these directions (sub-vectors) are the same as the one along the most unstable direction for the entire dynamic space. Therefore, even when we use only the dynamic variables $X_i(t) = \big(V_i(t), m_i(t), h_i(t), n_i(t)\big)$ for each neuron and use the vector $\mathbf{X}(t) = [X_1(t), \ldots, X_i(t), \ldots, X_N(t)]$ to compute the largest Lyapunov exponent, we can still obtain quantitatively correct results. We have confirmed that the pseudo-Lyapunov exponents are the same whether they are computed by using $[\mathbf{V}(t), \mathbf{m}(t), \mathbf{h}(t), \mathbf{n}(t)]$ or using $[\mathbf{V}(t), \mathbf{m}(t), \mathbf{h}(t), \mathbf{n}(t), \mathbf{G}(t)]$. Moreover, these results are consistent with the one computed by using the full dynamical vector $[\mathbf{V}(t), \mathbf{m}(t), \mathbf{h}(t), \mathbf{n}(t), \mathbf{G}(t), \widetilde{\mathbf{G}}(t)]$ with Mueller's method (Mueller 1995), as shown in Fig. 8 for those network systems we have been able to examine. This result provides strong evidence that our pseudo-Lyapunov exponents coincide with the standard Lyapunov exponents for our network dynamics.

In the mean field, large N limit, we find that the most unstable direction of the entire network system mainly lies in the subspace $[\mathbf{V}(t), \mathbf{m}(t), \mathbf{h}(t), \mathbf{n}(t)]$ as $N \to \infty$. This fact can be revealed by performing tests as shown in Fig. 9. First we define the *mean field limit* as the limit where the size of network $N \to \infty$, and each presynaptic input strength to any individual neuron scales as S/N. Clearly, each individual coupling strength $S/N \to 0$, as $N \to \infty$; but the total synaptic input remains finite. Here we compute the percentages of perturbation of the conductance terms $\mathbf{G}(t)$ and $\widetilde{\mathbf{G}}(t)$ (defined similarly as $\mathbf{V}(t)$) relative to the contribution of other variables in the perturbation for all neurons: $P_{\mathbf{G}} = \frac{\|\Delta \mathbf{G}\|}{\|\Delta \mathbf{X}\|}$ and $P_{\widetilde{\mathbf{G}}} = \frac{\|\Delta \widetilde{\mathbf{G}}\|}{\|\Delta \mathbf{X}\|}$, then take the mean field limit when the size of network is increased from $N = 10$ up to 10^4. It turns out that both percentages of $P_{\mathbf{G}}$ and $P_{\widetilde{\mathbf{G}}}$ in general are less than 1%, and they decrease nearly according to a power law as the size N increases, as shown in Fig. 9. These observations indicate that the dominant perturbation comes from the remaining variables in the dynamic vector, i.e., $[\mathbf{V}(t), \mathbf{m}(t), \mathbf{h}(t), \mathbf{n}(t)]$. Therefore, the most unstable direction of the entire system lies in the subspace spanned by these variables as $N \to \infty$ in the mean field limit of the network dynamics and we can use them as the smallest subset of variables to account for the network behavior.

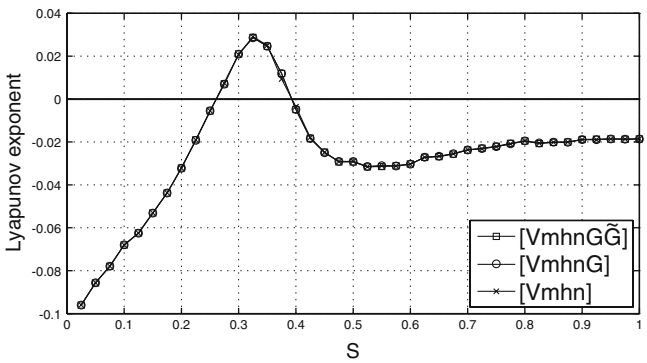

Fig. 8 The pseudo-Lyapunov exponent of the same network as the one in Fig. 3 versus the coupling strengths S. We show three cases with different dynamic variable combinations $[\mathbf{V}(t), \mathbf{m}(t), \mathbf{h}(t), \mathbf{n}(t), \mathbf{G}(t), \widetilde{\mathbf{G}}(t)]$ (*squares*), $[\mathbf{V}(t), \mathbf{m}(t), \mathbf{h}(t), \mathbf{n}(t), \mathbf{G}(t)]$ (*circles*), and $[\mathbf{V}(t), \mathbf{m}(t), \mathbf{h}(t), \mathbf{n}(t)]$ (*crosses*), respectively. The first case (*squares*) corresponds to the standard Lyapunov exponent for systems with jumps (Mueller 1995). Note that the curves for these three cases overlap. The total time for following the trajectories is sufficiently long (65536 ms) in order to obtain statistically convergent results for the pseudo-Lyapunov exponent

4.3 Firing rate

In many applications, it is often not necessary to resolve every single trajectory of all neurons in the system. For example, many physiological experiments (Koch 1999) only record the statistical properties of a subpopulation of neurons in the entire system, such as firing rate. For example, an experiment may only be concerned with the firing rate statistics or the ISI distribution aggregated for many neurons in the system over a long time. Although there is no convergence of the numerical solutions in the chaotic regime as discussed above, we can achieve accuracy in statistical quantities, such as the average firing rate.

First, we compare the statistical results of firing rate by using different time steps Δt for the RK4 solver from 2^{-7} to 2^{-4} ms. Figure 10(a) shows the average firing rate R, which is the number of firing events per neuron per second, averaged over the whole population of the neurons in the same network as in Fig. 3 for different values of coupling strength S. In the asynchronous regime ($0.025 \lesssim S \lesssim 0.263$ mS/cm^2), the firing rate increases slowly from 28 to 29 spikes/sec. When the network enters the chaotic regime ($0.263 \lesssim S \lesssim 0.395$ mS/cm^2), the firing rate firstly drops back to about 28 spikes/sec around $S \approx 0.275$ mS/cm^2, then grows rapidly as S increases, i.e., a strong gain across the chaotic regime. When the network becomes synchronous ($0.395 \lesssim S \lesssim 1.0$ mS/cm^2), the firing rate increases slowly from 44 to 48 spikes/sec.

Figure 10(b) shows the relative error in the average firing rate between the result with large time step ($\Delta t = 2^{-4} = 0.0625$ ms) and the result with small time step ($\Delta t = 2^{-9} = 0.001953125$ ms), which is defined as follows:

$$E^{\mathrm{R}} = |R^{\mathrm{small}} - R^{\mathrm{large}}|/R^{\mathrm{small}}. \tag{15}$$

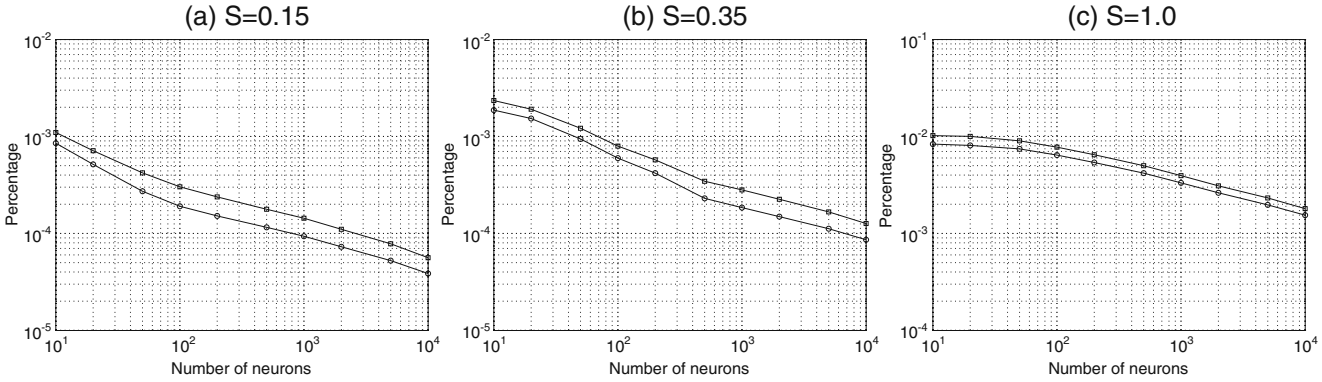

Fig. 9 Percentage of perturbation of conductance terms $\mathbf{G}(t)$ and $\widetilde{\mathbf{G}}(t)$ relative to the contribution of other dynamical variables for all neurons in an all-to-all connected network of N excitatory neurons driven by the feedforward input of a particular realization of a Poisson process with the rate $\omega = 50$ Hz versus the size N of the network from 10 up to 10^4. The plots from (a) to (c) show three cases with the coupling strength $S = 0.15$, 0.35, and 1.0 mS/cm^2 corresponding to an asynchronous, chaotic and synchronous regime, respectively. In each plot the *squares* correspond to the percentages of $\Delta\mathbf{G}$; the *circles* represent the percentages of $\Delta\widetilde{\mathbf{G}}$

We can achieve more than 2 digits accuracy in the average firing rate for all values of S, even in chaotic regime.

Finally we present a special test with a fixed coupling strength $S = 0.35$ mS/cm^2 and vary the input rate ω from 5 to 200 spikes/sec to study the gain function of the network. We find again that a chaotic regime exists for $30 \lesssim \omega \lesssim 70$ spikes/sec (Fig. 11(a)). Figure 11(b) shows the average firing rate R with different time steps Δt from 2^{-7} to 2^{-4} ms. In Fig. 11(c), we show that there is also more than 2 digits accuracy in the average firing rate for all values of ω. Again, this indicates that we can achieve accuracy in the statistical quantification in the chaotic regime.

4.4 Network with a high-order kinetics in conductance

To present evidence that chaos is not arising from threshold dynamics at V^{th}, we extend the study of the HH neuronal network dynamics further by using a continuous function (in Eq. (21) below) to describe the dynamics of synaptic interactions (Compte et al. 2003) (only the feedforward inputs have jump variables, as shown in Eq. (20) below). Therefore, there is no hard threshold V^{th} as in the model in Subsection 2.1. Moreover, in order to evolve the network dynamics by using the standard RK4 scheme *without* the spike-spike correction procedure, we use a high-order kinetics in conductance to make it sufficiently smooth as demanded by the use of the RK4 scheme. Then the synaptic interactions in this system are no longer event-driven and our numerical method can have a fourth-order accuracy. For simplicity, we again study an all-to-all connected network of 100 excitatory neurons and omit the index Q labeling the types of conductances. The dynamics of $G_i(t)$ are governed by

$$\frac{d}{dt}G_i(t) = -\frac{G_i(t)}{\sigma_{\text{r}}} + G_{1i}(t), \tag{16}$$

$$\frac{d}{dt}G_{1i}(t) = -\frac{G_{1i}(t)}{\sigma_{\text{r}}} + G_{2i}(t), \tag{17}$$

$$\frac{d}{dt}G_{2i}(t) = -\frac{G_{2i}(t)}{\sigma_{\text{r}}} + G_{3i}(t), \tag{18}$$

$$\frac{d}{dt}G_{3i}(t) = -\frac{G_{3i}(t)}{\sigma_{\text{r}}} + G_{4i}(t), \tag{19}$$

$$\frac{d}{dt}G_{4i}(t) = -\frac{G_{4i}(t)}{\sigma_{\text{r}}} + \sum_{j\neq i} S_{i,j}\, g\left(V_j^{\text{pre}}\right) + \sum_k F_i\, \delta\left(t - T_{i,k}^{\text{F}}\right), \tag{20}$$

where

$$g\left(V_j^{\text{pre}}\right) = \frac{1}{1 + \exp\left(-\left(V_j^{\text{pre}} - 20\right)/2\right)}. \tag{21}$$

We evolve the network dynamics by solving Eqs. (16)–(21) coupled with Eqs. (1)–(5). Note that for a fixed realization of the input, the system is deterministic. For this system, one expects that our numerical method should be formally fourth-order accurate. However, when we perform simulations of the network driven by the same realization of stochastic feedforward input for synaptic coupling strength S ranging from 0.025 to 1.0 mS/cm^2, we find again that a chaotic regime exists for $0.25 \lesssim S \lesssim 0.4$ mS/cm^2 (Fig. 12(a)). For this regime, there is no classical trajectory convergence as shown in Fig. 13.

We have also confirmed that the pseudo-Lyapunov exponents are the same whether they are computed by using partial dynamical variables $[\mathbf{V}(t), \mathbf{m}(t), \mathbf{h}(t), \mathbf{n}(t)]$ or using all continuous dynamical variables $[\mathbf{V}(t), \mathbf{m}(t), \mathbf{h}(t), \mathbf{n}(t), \mathbf{G}(t), \mathbf{G}_1(t), \mathbf{G}_2(t), \mathbf{G}_3(t)]$. Moreover, these results are consistent with the one computed by using the full dynamical vector $[\mathbf{V}(t), \mathbf{m}(t), \mathbf{h}(t), \mathbf{n}(t), \mathbf{G}(t), \mathbf{G}_1(t), \mathbf{G}_2(t), \mathbf{G}_3(t), \mathbf{G}_4(t)]$ with Mueller's method, as shown in Fig. 12(b). For this smooth pulse-coupled dynamics (i.e. no hard threshold), the pseudo-Lyapunov exponents again coincide with those of the standard one, i.e., using the full set of dynamical variables.

To find whether the dynamics of a neuron that receives the feedforward input plus the spikes from other neurons in this type of HH network can be chaotic or not, we again employ the notion of a "test" neuron to calculate the pseudo-Lyapunov exponent of a single test neuron. In Fig. 12(c), we show that the pseudo-Lyapunov exponent of a single test neuron remains negative for any value of S, which indicates that the dynamics of a single test neuron in this network is not chaotic.

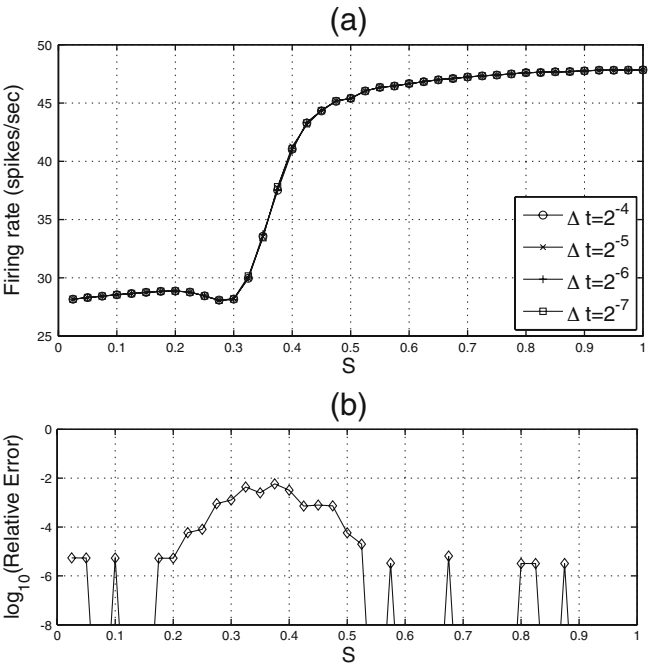

Fig. 10 (**a**): Average firing rate of the same network as the one in Fig. 3 versus the coupling strengths S by using different time steps $\Delta t = 2^{-7}$ to 2^{-4} ms. (**b**): The relative error in the average firing rate between the result with a large time step ($\Delta t = 2^{-4}$ ms) and the result with a small time step ($\Delta t = 2^{-9}$ ms) versus S. Note that there are several points of S for which the relative error are not plotted in Panel (**b**) since the results of the average firing rate using two different time steps are identical at these points and the relative errors vanish. The total time is 65536 ms

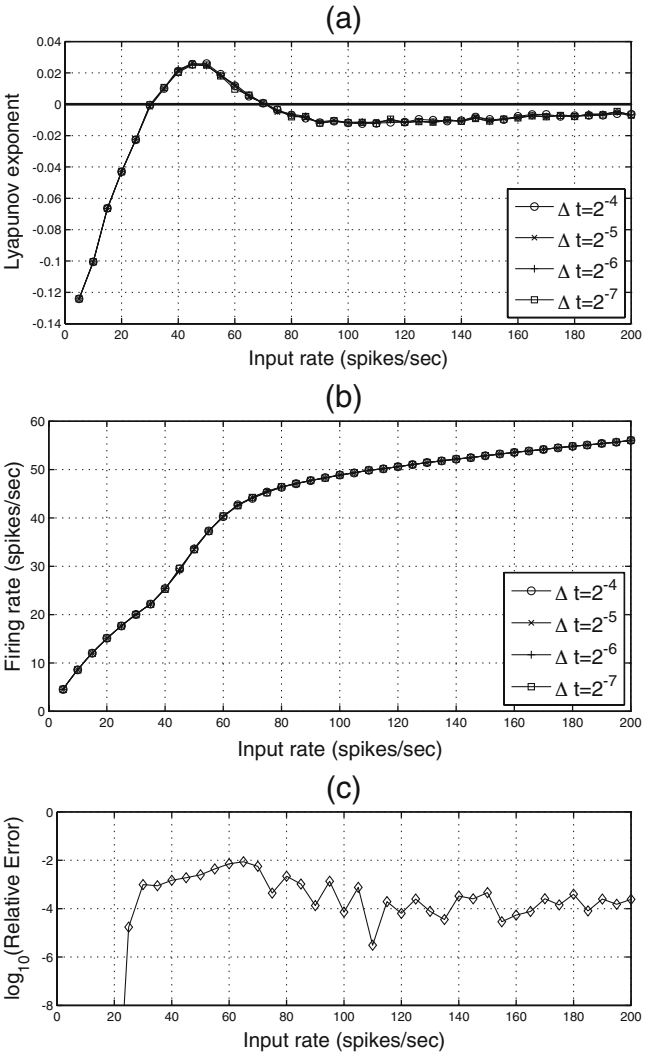

Fig. 11 (**a**) The pseudo-Lyapunov exponent of the same network as the one in Fig. 3 versus the input rate ω for the coupling strength $S = 0.35$ mS/cm^2 by using different time steps $\Delta t = 2^{-7}$ to 2^{-4} ms. (**b**): Average firing rate versus the input rate ω. (**c**): The relative error in the average firing rate between the result with a large time step ($\Delta t = 2^{-4}$ ms) and the result with a small time step ($\Delta t = 2^{-9}$ ms) versus ω. Note that there are several points of ω (≤ 15 spikes/sec) for which the relative error are not plotted in Panel (**c**) since the results of the average firing rate using two different time steps are identical at these points and the relative errors vanish. The total time is 65536 ms

As shown in Fig. 13, our method can achieve fourth-order numerical convergence when $S = 0.15$ (asynchronous state) and 1.0 mS/cm^2 (synchronous state). However, for $S = 0.35$ mS/cm^2, there is no convergence of the solutions. This non-convergence is consistent with the fact that the largest Lyapunov exponent is positive in the chaotic dynamics.

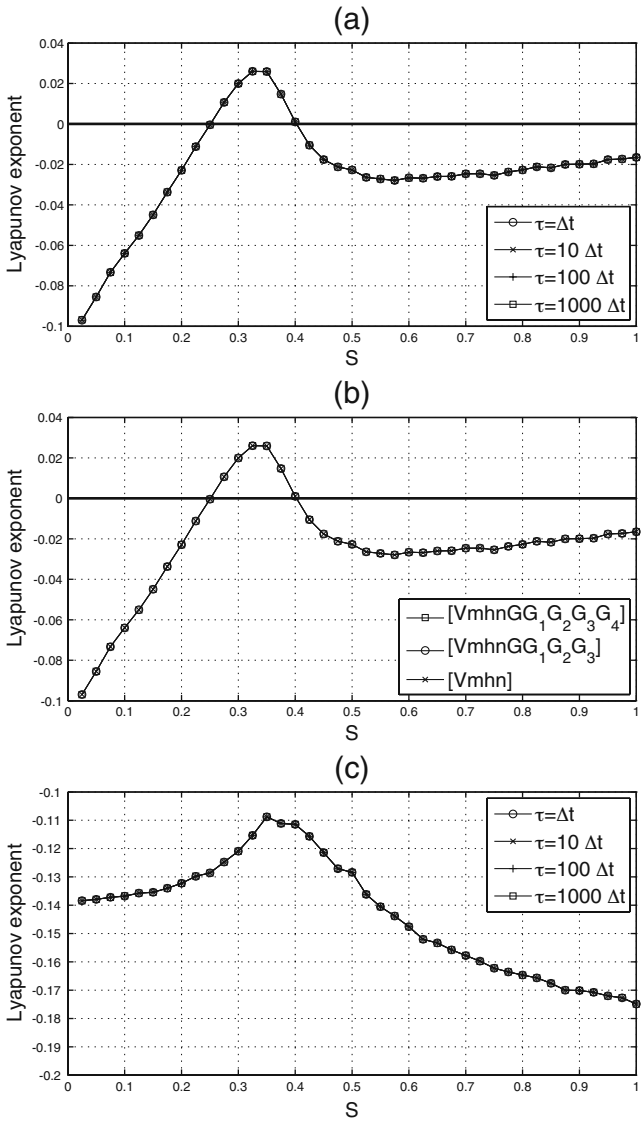

Fig. 12 (**a**): The pseudo-Lyapunov exponent of the network with a high-order kinetics in conductance term versus the coupling strengths S. Note that all the curves for different values of τ essentially overlap. (**b**): We show three cases with different dynamic variable combinations $[\mathbf{V}(t), \mathbf{m}(t), \mathbf{h}(t), \mathbf{n}(t), \mathbf{G}(t), \mathbf{G}_1(t), \mathbf{G}_2(t), \mathbf{G}_3(t), \mathbf{G}_4(t)]$ (*squares*), $[\mathbf{V}(t), \mathbf{m}(t), \mathbf{h}(t), \mathbf{n}(t), \mathbf{G}(t), \mathbf{G}_1(t), \mathbf{G}_2(t), \mathbf{G}_3(t)]$ (*circles*), and $[\mathbf{V}(t), \mathbf{m}(t), \mathbf{h}(t), \mathbf{n}(t)]$ (*crosses*), respectively. Note that the curves for these three cases overlap. The first case (*squares*) corresponds to the standard Lyapunov exponent for systems with jumps (Mueller 1995). (**c**): The pseudo-Lyapunov exponent of a single test neuron in the network versus the coupling strengths S. In each plot we use different time steps τ for renormalization from 2^{-5} to 2^{-2} ms, but the time step Δt for the RK4 solver is the same (2^{-5} ms). Note that all the curves for different values of τ essentially overlap. The total time for following the trajectories is sufficiently long (65536 ms) in order to obtain statistically convergent results for the pseudo-Lyapunov exponent

4.5 Network with inhibitory neurons

We further address the question of how the above excitatory network results will be modified by the presence of inhibitory neurons. Therefore, we make another extension in the study of the HH neuronal network dynamics by adding inhibitory neurons into the network. Here, we consider an all-to-all connected network of 80 excitatory neurons and 20 inhibitory neurons with the discontinuous dynamics of the conductance term (Eqs. (6) and (7)). The stochastic feedforward input is the same as before with the input rate $\omega = 50$ Hz and other parameters are given in Appendix A.

In particular, we fix the coupling strength for inhibitory (excitatory) synapses onto excitatory (inhibitory) neurons $S^{EI} = S^{IE} = 0.1$ mS/cm^2 and vary the recurrent excitatory coupling strength S^{EE} ranging from 0.025 to 1.0 mS/cm^2 to perform four systematic scanning tests for four different values of recurrent inhibitory coupling strength $S^{II} = 0.1, 0.2$, 0.3 and 0.4 mS/cm^2, respectively. We find again a chaotic regime existing in the tests of $S^{II} = 0.1, 0.2$, and 0.3 mS/cm^2. As shown in Fig. 14(a), for the case of $S^{II} = 0.1$ mS/cm^2, the chaotic regime exists in $0.224 \lesssim S^{EE} \lesssim 0.447$ mS/cm^2 for which the pseudo-Lyapunov exponent is positive; for $S^{II} = 0.2$ mS/cm^2, the chaotic regime exists at all points of $0.025 \lesssim S^{EE} \lesssim 0.411$ mS/cm^2, and for $S^{II} = 0.3$ mS/cm^2, the chaotic regime exists at all points of $0.025 \lesssim S^{EE} \lesssim 0.345$ mS/cm^2. However, for $S^{II} = 0.4$ mS/cm^2, the pseudo-Lyapunov exponent is nega-

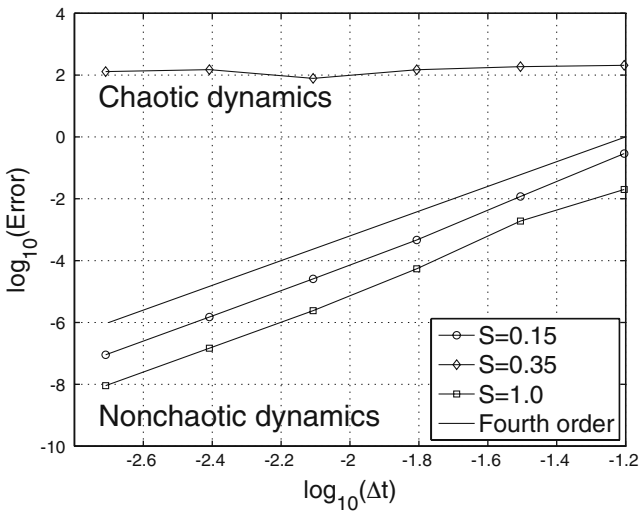

Fig. 13 The convergence tests are performed on the same network as the one in Fig. 12 by using the RK4 scheme with a final time of $t = 1024$ ms. In the plot we show three cases with the coupling strength $S = 0.15$ (*circles*), 0.35 (*crosses*) and 0.7 mS/cm^2 (*squares*), respectively. The solid line indicates the slope for the fourth order convergence

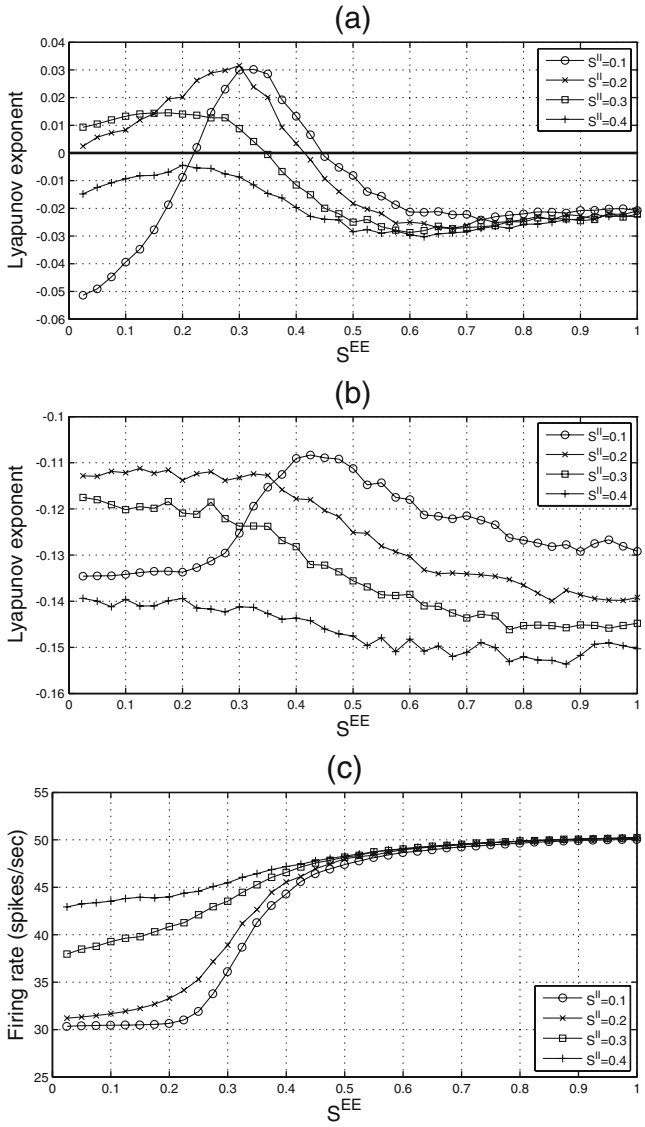

Fig. 14 (**a**): The pseudo-Lyapunov exponent of the network with 80 excitatory and 20 inhibitory neurons versus the coupling strengths S^{EE} between the excitatory neurons; (**b**): The pseudo-Lyapunov exponent of a single test neuron in the network versus the coupling strengths S^{EE}; (**c**): Average firing rate of the network versus the coupling strengths S^{EE}. In each plot, we show four results of different inhibitory coupling strength $S^{II} = 0.1$ (*circles*), 0.2 (*crosses*), 0.3 (*squares*), and 0.4 mS/cm^2 (*pluses*). The total time for following the trajectories is sufficiently long (65536 ms) in order to obtain statistically convergent results for the pseudo-Lyapunov exponent

tive for any value of S^{EE}, which indicates that there is no chaotic regime in this case.

Again, to address whether the dynamics of a neuron that receives the feedforward input plus the spikes from other neurons in this type of HH network can be chaotic or not, we employ the notion of a "test" neuron to calculate the pseudo-Lyapunov exponent of a single neuron. In Fig. 14(b), we show that the pseudo-Lyapunov exponent of a single test neuron is negative for any values of S^{EE} and S^{II}, which indicates that the dynamics of a single test neuron in this network is not chaotic. In Fig. 14(c), we also show that the average firing rates for all cases are monotonically increasing as S^{EE} increases.

As shown in Fig. 15(a), when $S^{II} = 0.1$ mS/cm^2, our numerical method can achieve fourth-order accuracy for both nonchaotic cases $S^{EE} = 0.15$ and 1.0 mS/cm^2. However, for $S^{EE} = 0.35$ mS/cm^2, consistent with the chaotic dynamics, we cannot achieve convergence of the solutions. For $S^{II} = 0.2$ mS/cm^2 as shown in Fig. 15(b), there is no convergence for either cases $S^{EE} = 0.15$ or 0.35 mS/cm^2 as they are in chaotic regime (Fig. 14(a)). Only for the case of $S^{EE} = 1.0$ mS/cm^2, we can achieve numerical convergence of the solutions. As shown in Fig. 15(c), when $S^{II} = 0.3$ mS/cm^2, there is convergence of the solutions for both nonchaotic cases $S^{EE} = 0.35$ and 1.0 mS/cm^2, but not for the case $S^{EE} = 0.15$ mS/cm^2. In Fig. 15(d), when $S^{II} = 0.4$ mS/cm^2, we can achieve convergence of the solutions for all three cases as they are in nonchaotic regime. In summary, our numerical method for evolving the network dynamics are consistent with the dynamical regimes of the network as very well indicated by the pseudo-Lyapunov exponent.

4.6 Network with heterogeneous coupling strengths

Finally, we present a study of the HH neuronal network dynamics with heterogeneous coupling strengths and show the robustness of the proposed method. Here, we again consider an all-to-all connected network of 80 excitatory neurons and 20 inhibitory neurons with the discontinuous dynamics of the conductance term (Eqs. (6) and (7)). The stochastic feedforward input is the same as before with the input rate $\omega = 50$ Hz and other parameters are given in Appendix A. In particular, we generate a $N \times N$ random matrix $\mathbf{A}$ with exponentially distributed random elements $A_{i,j}$. Then the coupling strength for the jth neuron's synapses onto the ith neuron is given by $S_{i,j} = A_{i,j} S^{Q}_{i,j}$, in which $S^{Q}_{i,j}$ is a constant S^{Q}/N^{Q} with N^{Q} being the total number of Q-type neurons in the network, as we define in Section 2.

Here we fix the parameter of the coupling strength for inhibitory (excitatory) synapses onto excitatory (inhibitory) neurons $S^{EI} = S^{IE} = 0.05$ mS/cm^2 and vary the parameter of the recurrent excitatory coupling strength S^{EE} ranging from 0.01 to 0.4 mS/cm^2 to perform four systematic scanning tests for four different parameter values of recurrent inhibitory coupling strength $S^{II} = 0.1, 0.2, 0.3$ and 0.4 mS/cm^2,

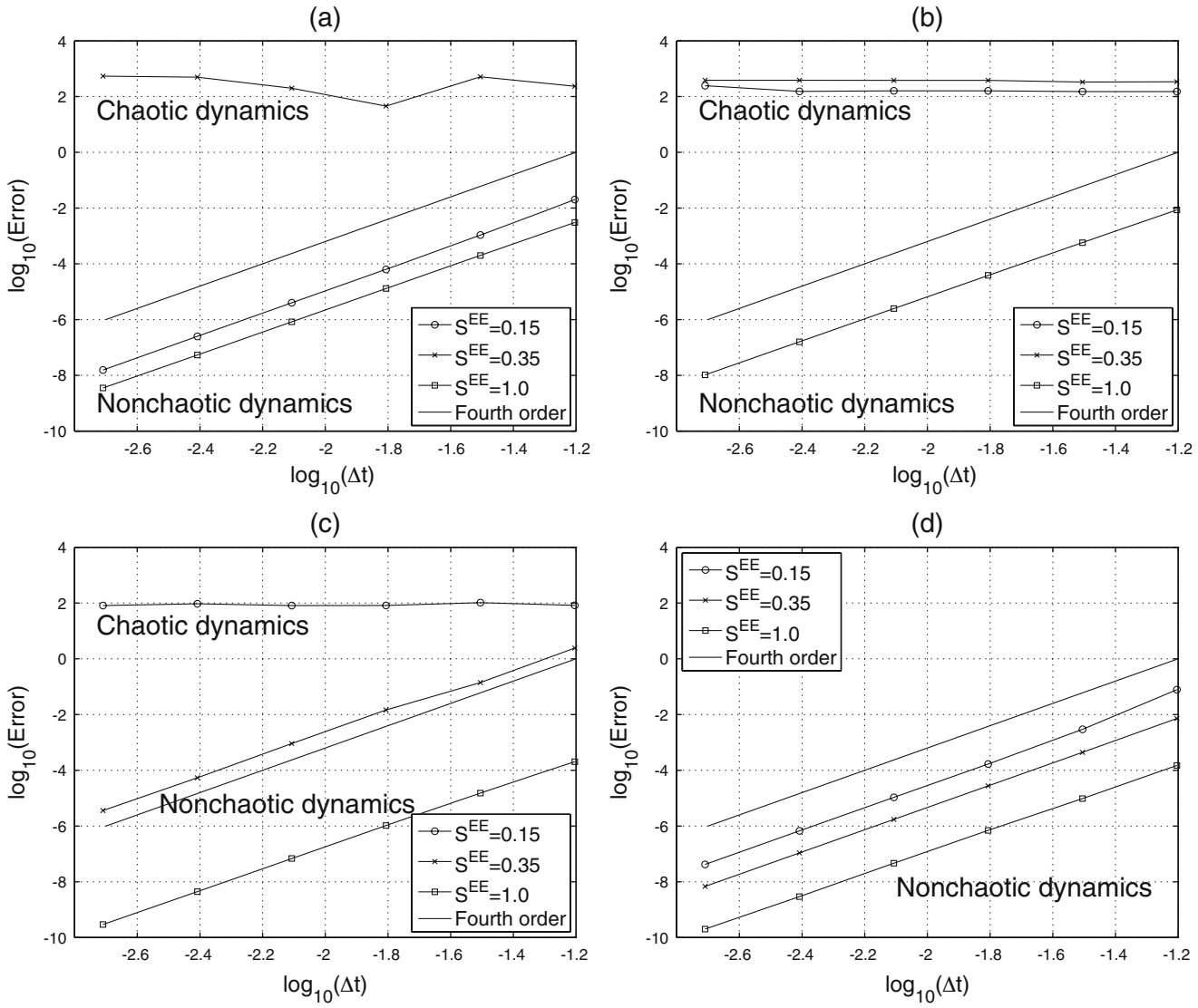

Fig. 15 The convergence tests are performed on the same network as the one in Fig. 14 by using the RK4 scheme with a final time of $t = 1024$ ms for two different inhibitory coupling strength (**a**) $S^{II} = 0.1$, (**b**) 0.2, (**c**) 0.3, and (**d**) 0.4 mS/cm^2. In each plot, we show three cases with the coupling strength $S^{EE} = 0.15$ (*circles*), 0.35 (*crosses*) and 1.0 mS/cm^2 (*squares*), respectively. The *solid line* indicates the slope for the fourth order convergence

respectively. We find a chaotic regime existing in all tests. As shown in Fig. 16(a), when $S^{II} = 0.1$ mS/cm^2, the chaotic regime exists at all points of $0.01 \lesssim S^{EE} \lesssim 0.174$ mS/cm^2, but for the other cases of $S^{II} = 0.2, 0.3$ and 0.4 mS/cm^2, the chaotic regime exists roughly in the intermediate regime $0.085 \lesssim S^{EE} \lesssim 0.165$ mS/cm^2 for which the pseudo-Lyapunov exponent is positive.

In Fig. 16(b), we show that the pseudo-Lyapunov exponents of a single test neuron are negative for any values of S^{EE} and S^{II}, which indicates that the dynamics of a single test neuron in this network is not chaotic. In Fig. 16(c), we also show that the average firing rates for all cases are monotonically increasing as S^{EE} increases.

As shown in Fig. 17(a), when $S^{II} = 0.1$ mS/cm^2, our numerical method cannot achieve fourth-order accuracy for both chaotic cases $S^{EE} = 0.05$ and 0.14 mS/cm^2. However, for $S^{EE} = 0.4$ mS/cm^2, consistent with the nonchaotic dynamics, we can achieve convergence of the solutions. For $S^{II} = 0.2$ mS/cm^2 as shown in Fig. 17(b), there is no convergence for the case $S^{EE} = 0.14$ mS/cm^2 as it is in chaotic regime (Fig. 16(a)). But for the cases of $S^{EE} = 0.05$ and 0.4 mS/cm^2, we can achieve numerical convergence of the solutions. Since the results of the other two cases, $S^{II} = 0.3$ and 0.4 mS/cm^2, are similar to the one of $S^{II} = 0.2$ mS/cm^2, we omit the plots for these cases

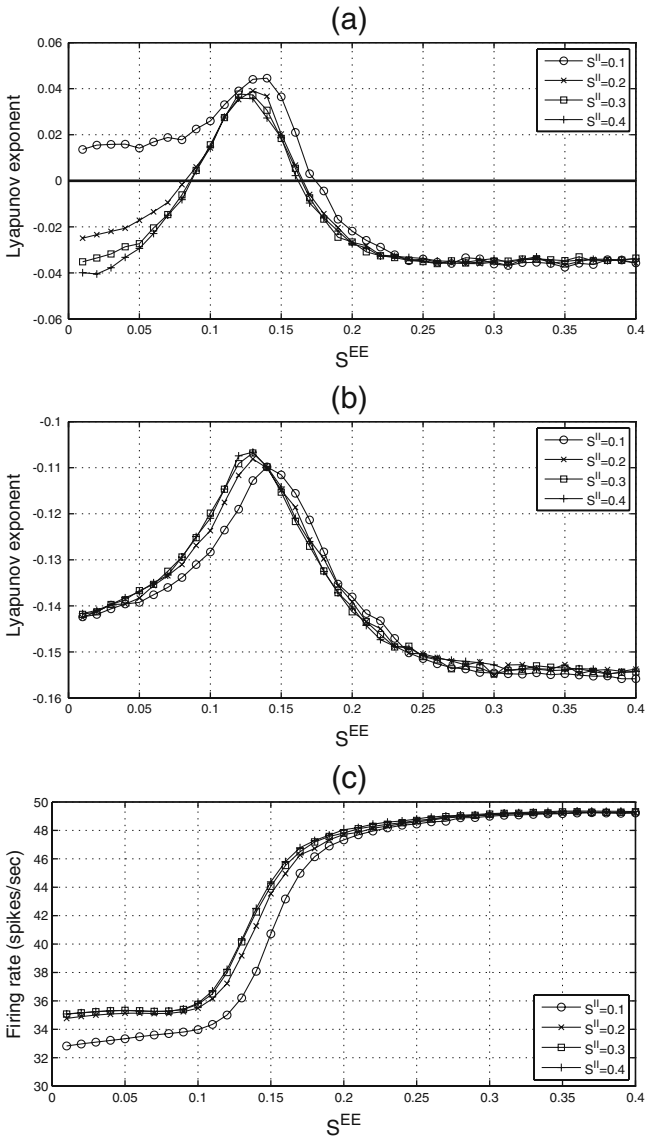

Fig. 16 (**a**): The pseudo-Lyapunov exponent of the network with heterogeneous coupling strengths with 80 excitatory and 20 inhibitory neurons versus the coupling strength parameter S^{EE} between the excitatory neurons; (**b**): The pseudo-Lyapunov exponent of a single test neuron in the network versus the coupling strength parameter S^{EE}; (**c**): Average firing rate of the network versus the coupling strength parameter S^{EE}. In each plot, we show four results of different inhibitory coupling strength $S^{II} = 0.1$ (*circles*), 0.2 (*crosses*), 0.3 (*squares*), and 0.4 mS/cm^2 (*pluses*). The total time for following the trajectories is sufficiently long (65536 ms) in order to obtain statistically convergent results for the pseudo-Lyapunov exponent

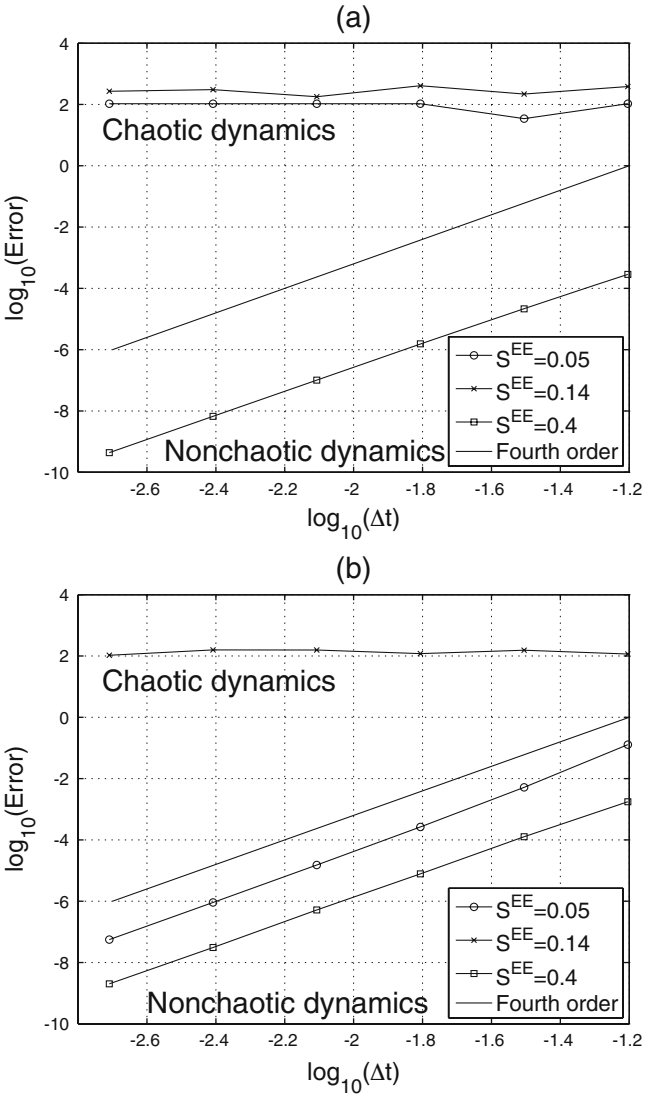

Fig. 17 The convergence tests are performed on the same network as the one in Fig. 16 by using the RK4 scheme with a final time of $t = 1024$ ms for two different inhibitory coupling strength (**a**) $S^{II} = 0.1$ and (**b**) 0.2 mS/cm^2. In each plot, we show three cases with the coupling strength $S^{EE} = 0.05$ (*circles*), 0.14 (*crosses*) and 0.4 mS/cm^2 (*squares*), respectively. The *solid line* indicates the slope for the fourth order convergence. Since the results of the other two cases $S^{II} = 0.3$ and 0.4 mS/cm^2 are similar to the one of $S^{II} = 0.2$ mS/cm^2, we omit the plots for these cases here

here. In summary, our numerical method for evolving the network dynamics with heterogeneous coupling strengths are consistent with the dynamical regimes of the network as very well indicated by the pseudo-Lyapunov exponent.

5 Conclusion

We have presented a numerical study of the network dynamics of HH neurons with Poisson spike inputs and found three typical dynamical regimes—the asynchronous, chaotic and synchronous ones as the synaptic coupling strength varies from weak to strong. In the nonchaotic (asynchronous or synchronous) dynamical regimes, i.e., the weak or strong coupling limits, we can

achieve good numerical convergence of the solution in the trajectory-wise sense by using our numerical methods. Therefore, in these regimes the solutions are reliable. For the chaotic dynamical regime with an intermediate strong coupling, there is no numerical convergence of the solution and only statistical quantifications of the numerical results are reliable, such as the average firing rate. We also emphasize that the chaos is a network property in a certain regime and the dynamics of a test neuron that receives the feedforward input plus the spikes from other neurons in the network is usually not chaotic.

We apply and extend several tools from the dynamical system's theory, such as measuring the largest Lyapunov exponent and the power spectrum analysis of voltage traces to characterize the types of the network behavior. In particular, we propose so-called pseudo-Lyapunov exponent adapted from the classical definition by excluding the discontinuous variables from the trajectory vector. In the nonchaotic dynamical regimes, the pseudo-Lyapunov exponent is negative. The chaotic regime is signified by a positive pseudo-Lyapunov exponent. The numerical results of the pseudo-Lyapunov exponent using the new definition are consistent with the dynamical regimes of the network very well. Furthermore, our numerical studies also present strong evidence that, for HH network dynamics, the values of pseudo-Lya-punov exponents coincide with those of the standard Lyapunov exponents. It will be interesting to further investigate whether these two notions are mathematically equivalent for HH network dynamics. This will further extend classical results about the Lyapunov exponents to thresholded, pulse-coupled network dynamics.

Most of the results presented in this article were obtained for networks of $N = 100$ neurons, but increasing the size of the network does not change our conclusions. In addition, although we have focused on the models with the stochastic feedforward input and shown the corresponding numerical results in previous section, similar phenomena appear when we use deterministic models with a continuous type of feedforward input. There are also three dynamical regimes corresponding to the asynchronous, chaotic and synchronous states of the network as the coupling strength increases (Sun et al. 2009).

Acknowledgements The work was supported by NSF grants DMS-0506396, DMS-0507901 and a grant from the Swartz foundation.

Appendix A: Parameter values for the Hodgkin-Huxley equations

Parameter values or ranges and function definitions of the Hodgkin-Huxley model are as follows (Dayan and Abbott 2001):

$$
\begin{aligned}
G_{\mathrm{Na}} &= 120\ \mathrm{mS/cm^2},\quad V_{\mathrm{Na}} = 50\ \mathrm{mV},\\
G_{\mathrm{K}} &= 36\ \mathrm{mS/cm^2},\quad V_{\mathrm{K}} = -77\ \mathrm{mV},\\
G_{\mathrm{L}} &= 0.3\ \mathrm{mS/cm^2},\quad V_{\mathrm{L}} = -54.387\ \mathrm{mV},\\
C &= 1\mu\ \mathrm{F/cm^2},\quad V_{\mathrm{G}}^{\mathrm{E}} = 0\ \mathrm{mV},\quad V_{\mathrm{G}}^{\mathrm{I}} = -80\ \mathrm{mV},\\
F^{\mathrm{E}} &= 0.05 \sim 0.1\ \mathrm{mS/cm^2},\quad S^{\mathrm{E}} = 0.05 \sim 1.0\ \mathrm{mS/cm^2},\\
F^{\mathrm{I}} &= 0.01 \sim 0.05\ \mathrm{mS/cm^2},\quad S^{\mathrm{I}} = 0.05 \sim 1.0\ \mathrm{mS/cm^2},\\
\sigma_{\mathrm{r}}^{\mathrm{E}} &= 0.5\ \mathrm{ms},\quad \sigma_{\mathrm{d}}^{\mathrm{E}} = 3.0\ \mathrm{ms},\\
\sigma_{\mathrm{r}}^{\mathrm{I}} &= 0.5\ \mathrm{ms},\quad \sigma_{\mathrm{d}}^{\mathrm{I}} = 7.0\ \mathrm{ms},\\
\alpha_m(V) &= 0.1(V+40)/(1-\exp(-(V+40)/10)),\\
\beta_m(V) &= 4\exp(-(V+65)/18),\\
\alpha_h(V) &= 0.07\exp(-(V+65)/20),\\
\beta_h(V) &= 1/(1+\exp(-(35+V)/10)),\\
\alpha_n(V) &= 0.01(V+55)/(1-\exp(-(V+55)/10)),\\
\beta_n(V) &= 0.125\exp(-(V+65)/80).
\end{aligned}
$$

Appendix B: Numerical method for a single neuron

Here we provide details of the numerical method for evolving the dynamics of a single neuron. For simplicity, we use vector X_i to represent all the variables in the solution of the ith neuron:

$$X_i(t) = \big(V_i(t), m_i(t), h_i(t), n_i(t), G_i^{\mathrm{Q}}(t), \widetilde{G}_i^{\mathrm{Q}}(t)\big).$$

Given an initial time t_0 and time step Δt, initial values $X_i(t_0)$, and spike times $T_{i,k}^{\mathrm{F}}$ and $T_{j\neq i,k}^{\mathrm{S}}$ from the rest of the network, our method computes a numerical solution of all variables $X_i(t_0+\Delta t)$ as well as the intervening spike times $T_{i,k}^{\mathrm{S}}$ (if any occurred) for the ith neuron as follows:

Algorithm 1. *(Single neuron scheme)*

Step 1: Input: an initial time t_0, a time step Δt, a set of spike times $T_{i,k}^{\mathrm{F}}$ and $T_{j\neq i,k}^{\mathrm{S}}$ and associated strengths F_i^{Q} and $S_{i,j}^{\mathrm{Q}}$.

Step 2: Consider the time interval $[t_0, t_0+\Delta t]$. Let M denote the total number of feedforward and presynaptic spikes within this interval. Sort these spikes into an increasing list of M spike times T_m^{sorted} with corresponding spike strengths $S_m^{\mathrm{sorted,Q}}$. In addition, we extend this

notation such that $T_0^{\text{sorted}} := t_0$, $T_{M+1}^{\text{sorted}} := t_0 + \Delta t$ *and* $S_0^{\text{sorted,Q}} = S_{M+1}^{\text{sorted,Q}} := 0$.

Step 3: For $m = 1, \ldots, M+1$, *advance the equations for the HH neuron model and its conductances (Eqs. (1)–(7)) from* T_{m-1}^{sorted} *to* T_m^{sorted} *using the standard RK4 scheme to obtain* $X_i(T_m^{\text{sorted}})$; *Then, update the conductance* $\widetilde{G}_i^{\text{Q}}(T_m^{\text{sorted}})$ *by adding the appropriate strengths* $S_m^{\text{sorted,Q}}$.

Step 4: If the calculated values for $V_i(T_m^{\text{sorted}})$ *are each less than* V^{th}, *then we can accept* $X_i(T_{M+1}^{\text{sorted}})$ *as the solution* $X_i(t_0 + \Delta t)$. *We update* $t_0 \leftarrow t_0 + \Delta t$ *and return to step 2 and continue.*

Step 5: Otherwise, let $V_i(T_m^{\text{sorted}})$ *be the first calculated voltage greater than* V^{th}. *We know that the* ith *neuron fired somewhere during the interval* $[T_{m-1}^{\text{sorted}}, T_m^{\text{sorted}}]$.

Step 6: In this case we use a high-order polynomial interpolation to find an approximation of the spike time t^{fire} *in the interval* $[T_{m-1}^{\text{sorted}}, T_m^{\text{sorted}}]$. *For example, we can use the numerical values of* $V_i(T_{m-1}^{\text{sorted}})$, $V_i(T_m^{\text{sorted}})$, $\frac{d}{dt}V_i(T_{m-1}^{\text{sorted}})$, $\frac{d}{dt}V_i(T_m^{\text{sorted}})$ *to form a cubic polynomial. We record* t^{fire} *as the* $(k+1)$th *postsynaptic spike time* $T_{i,k+1}^{\text{S}}$ *of the* ith *neuron. We update* $t_0 \leftarrow t_0 + \Delta t$ *and return to step 2 and continue.*

Appendix C: Numerical method for the HH network

Here we briefly outline an algorithm which accounts for spike-spike interactions, and can accurately evolve recurrent HH networks governed by Eqs. (1)–(7).

Algorithm 2. *(Network model scheme)*

Step 1: Given initial values initial values $X_i(t_0)$ *and feedforward input spike times* $T_{i,k}^{\text{F}}$ *for all i, we can apply Algorithm 1 and time step* Δt *to obtain an estimate of neuronal trajectories on the interval* $[t_0, t_0 + \Delta t]$.

Step 2: We use this rough estimate to classify the neurons into two groups $\mathscr{A}^{\text{spike}}$, $\mathscr{A}^{\text{quiet}}$*—those that are estimated to fire within* $[t_0, t_0 + \Delta t]$ *and those that are not.*

Step 3: We sort the approximate spike times of neurons within $\mathscr{A}^{\text{spike}}$ *into a list* $\mathscr{T}$ *with corresponding coupling strengths* $\mathscr{S}$.

Step 4: We use the feedforward spikes $T_{i,k}^{\text{F}}$ *as well as the approximate spike times* $\mathscr{T}$ *and Algorithm 1 and the same time step* Δt *to correct the neuronal trajectories of the subnetwork* $\mathscr{A}^{\text{spike}}$ *over the interval* $[t_0, t_0 + \Delta t]$, *and obtain a more accurate approximation to the spike times* $\mathscr{T}$. *This spike-spike correction procedure is equivalent to stepping through the list* $\mathscr{T}$ *and computing the effect of each spike on all future spikes. We step through this correction process until the neuronal trajectories and spike times of neurons in* $\mathscr{A}^{\text{spike}}$ *converge.*

Step 5: Finally we use the corrected estimates of the spike times $\mathscr{T}$ *as well as the feedforward spikes* $T_{i,k}^{\text{F}}$ *and Algorithm 1 and time step* Δt *to evolve the remainder of the neurons* $\mathscr{A}^{\text{quiet}}$ *from* t_0 *to* $t_0 + \Delta t$.

References

Aihara, K., & Matsumoto, G. (1986). Chaotic oscillations and bifurcations in squid giant axons. In *Chaos, nonlinear science: Theory and applications*. Manchester: Manchester University Press.

Cai, D., Rangan, A. V., & McLaughlin, D. W. (2005). Architectural and synaptic mechanisms underlying coherent spontaneous activity in v1. *Proceedings of the National Academy of Sciences (USA), 102*, 5868–5873.

Campbell, D., & Rose, H. (Eds.) (1983). Order in chaos. *Physica D, 7*, 1–362.

Compte, A., Sanchez-Vives, M. V., McCormick, D. A., & Wang, X. J. (2003). Cellular and network mechanisms of slow oscillatory activity (< 1 Hz) and wave propagations in a cortical network model. *Journal of Neurophysiology, 89*, 2707–2725.

Dayan, P., & Abbott, L. F. (2001). *Theoretical neuroscience: Computational and mathematical modeling of neural systems*. Cambridge: MIT.

Guckenheimer, J., & Oliva, R. A. (2002). Chaos in the Hodgkin-Huxley model. *SIAM Journal on Applied Dynamical Systems, 1*, 105–114.

Hansel, D., Mato, G., Meunier, C., & Neltner, L. (1998). On numerical simulations of integrate-and-fire neural networks. *Neural Computation, 10*, 467–483.

Hansel, D., & Sompolinsky, H. (1992). Synchronization and computation in a chaotic neural network. *Physical Review Letters, 68*, 718–721.

Hansel, D., & Sompolinsky, H. (1996). Chaos and synchrony in a model of a hypercolumn in visual cortex. *Journal of Computational Neuroscience, 3*, 7–34.

Hodgkin, A. L., & Huxley, A. F. (1952). A. quantitative description of membrane current and its application to conduction and excitation in nerve. *Journal of Physiology, 117*, 500–544.

Koch, C. (1999). *Biophysics of computation*. Oxford: Oxford University Press.

Kosmidis, E. K., & Pakdaman, K. (2003). An analysis of the reliability phenomenon in the FitzHugh-Nagumo model. *Journal of Computational Neuroscience, 14*, 5–22.

Lin, K. (2006). Entrainment and chaos in a pulse-driven Hodgkin-Huxley oscillator. *SIAM Journal on Applied Dynamical Systems, 5*, 179–204.

Mainen, Z., & Sejnowski, T. (1995). Reliability of spike timing in neocortical neurons. *Science, 268*, 1503–1506.

Mattia, M., & Del Giudice, P. (2000). Efficient event-driven simulation of large networks of spiking neurons and dynamical synapses. *Neural Computation, 12*, 2305–2329.

McLaughlin, D., Shapley, R., Shelley, M., & Wielaard, J. (2000). A neuronal network model of macaque primary visual cortex (V1): Orientation selectivity and dynamics in the input layer 4Cα. *Proceedings of the National Academy of Sciences USA, 97*, 8087–8092.

Mueller, P. (1995). Calculation of Lyapunov exponents for dynamic systems with discontinuities. *Chaos, Solitons & Fractals, 5*, 1671–1681.

Ott, E. (1993). *Chaos in dynamical systems*. New York: Cambridge University Press.

Parker, T. S., & Chua, L. O. (1989). *Practical numerical algorithms for chaotic systems*. New York: Springer.

Rangan, A. V., & Cai, D. (2007). Fast numerical methods for simulating large-scale integrate-and-fire neuronal networks. *Journal of Computational Neuroscience, 22*, 81–100.

Rangan, A. V., Cai, D., & McLaughlin, D. W. (2005). Modeling the spatiotemporal cortical activity associated with the line-motion illusion in primary visual cortex. *Proceedings of the National Academy of Sciences (USA), 102*, 18793–18800.

Reutimann, J., Giugliano, M., & Fusi, S. (2003). Event-based simulation of spiking neurons with stochastic dynamics. *Neural Computation, 15*, 811–830.

Rudolph, M., & Destexhe, A. (2007). How much can we trust neural simulation strategies? *Neurocomputing, 70*, 1966–1969.

Schuster, H. G., & Just, W. (2005). *Deterministic chaos*. Weinheim: Wiley-VCH Verlag.

Shelley, M. J., & Tao, L. (2001). Efficient and accurate time-stepping schemes for integrate-and-fire neuronal networks. *Journal of Computational Neuroscience, 11*, 111–119.

Somers, D., Nelson, S., & Sur, M. (1995). An emergent model of orientation selectivity in cat visual cortical simple cells. *Journal of Neuroscience, 15*, 5448–5465.

Sun, Y., Zhou, D., Rangan, A. V., & Cai, D. (2009). Library-based numerical reduction of the Hodgkin-Huxley neuron for network simulation. *Journal of Computational Neuroscience, 27*, 369–390.

Takens, F. (1981). Detecting strange attractors in turbulence. In *Dynamical systems and turbulence, lecture notes in mathematics* (Vol. 898). Berlin: Springer.

Troyer, T., Krukowski, A., Priebe N., & Miller, K. (1998). Contrast invariant orientation tuning in cat visual cortex with feedforward tuning and correlation based intracortical connectivity. *Journal of Neuroscience, 18*, 5908–5927.